SYNTHESIS AND CHARACTERIZATION OF MICROWAVE ASSISTED ACETYLATED RICE STARCH / POLYETHYLENE OXIDE (PEO) BLENDS

by

ONG KAI SIN

A project report submitted to the Department of Chemical Sciences

Faculty of Science

Universiti Tunku Abdul Rahman

In partial fulfilment of the requirements for the degree of

Bachelor of Science (Hons) Chemistry

October 2024

ABSTRACT

SYNTHESIS AND CHARACTERIZATION OF MICROWAVE ASSISTED ACETYLATED RICE STARCH / POLYETHYLENE OXIDE (PEO) BLENDS

ONG KAI SIN

Rice starch was modified via microwave-assisted esterification using acetic anhydride in the presence of iodine as the catalyst. An analysis of infrared spectra using Attenuated Total Reflectance-Fourier Transform Infrared (ATR-FTIR) spectroscopy showed a prominent peak at 1732 cm^{-1}, indicating the successful acetylation of rice starch due to the presence of the carbonyl (C=O) group. The impact of the molar ratio of rice starch to acetic anhydride, the amount of iodine, and the reaction time on the degree of substitution (DS) of acetylated rice starch were investigated. The highest DS was achieved with a molar ratio of 1:4, using 0.25 mmol of iodine and a reaction time of two minutes. Solution casting was used to prepare polymer blends of poly(ethylene oxide) (PEO) with acetylated rice starch in various ratios. Differential scanning calorimetry (DSC) was utilized to investigate the isothermal crystallization, melting behavior, and miscibility of PEO in PEO/acetylated rice starch blends. The kinetics of isothermal crystallization of PEO in PEO/acetylated rice starch blends were analyzed using the Avrami equation. The Hoffman-Weeks equation

was used to estimate the equilibrium melting temperatures, T_m° of PEO and PEO/acetylated rice starch blends. The Nishi-Wang equation was used to investigate the miscibility of PEO and acetylated rice starch. Positive values of polymer-polymer interaction parameter, χ_{12} for the PEO/acetylated rice starch blends were obtained, indicating that the blends were immiscible.

ABSTRAK

Kanji beras telah diubah suai melalui esterifikasi dibantu gelombang mikro menggunakan anhidrida asetik dengan kehadiran iodin sebagai pemangkin. Analisis spektrum inframerah menggunakan spektroskopi Attenuated Total Reflectance-Fourier Transform Infrared (ATR-FTIR) menunjukkan puncak yang ketara pada 1732 cm^{-1}, menunjukkan kejayaan asetilasi kanji beras disebabkan kehadiran kumpulan karbonil (C=O). Kesan nisbah molar kanji beras kepada anhidrida asetik, jumlah iodin, dan masa tindak balas terhadap tahap penggantian (DS) kanji beras asetilasi telah disiasat. DS tertinggi dicapai dengan nisbah molar 1:4, menggunakan 0.25 mmol iodin dan masa tindak balas selama dua minit. Teknik pelarutan digunakan untuk mencipta campuran polimer poli(etilena oksida) (PEO) dengan kanji asetilasi beras dalam pelbagai nisbah. Kalorimetri imbasan perbezaan (DSC) digunakan untuk mengkaji penghabluran isoterma, tingkah laku peleburan, dan kebolehcampuran PEO dalam campuran PEO/kanji asetilasi beras. Kinetik penghabluran isoterma PEO dalam campuran PEO/kanji asetilasi beras dianalisis menggunakan persamaan Avrami. Persamaan Hoffman-Weeks digunakan untuk menganggarkan suhu peleburan keseimbangan, T_m° bagi PEO dan campuran PEO/kanji asetilasi beras. Persamaan Nishi-Wang digunakan untuk mengkaji kebolehcampuran PEO dan kanji asetilasi beras. Nilai positif bagi parameter interaksi polimer-polimer, χ_{12} untuk campuran PEO/kanji asetilasi beras diperoleh, menunjukkan bahawa campuran tersebut tidak boleh bercampur.

ACKNOWLEDGEMENT

First and foremost, I would like to extend my heartfelt appreciation to my supervisor, Dr. Tan Shu Min, for her invaluable advice, guidance, and unwavering support throughout my final year project. Her persistence, determination, and depth of knowledge were incredibly helpful in assisting me with my research and thesis writing.

Furthermore, I would like to thank the laboratory officer, lab mates, and friends for their valuable assistance and insightful remarks on my project. In addition, I want to express my gratitude to my family for their wholehearted financial and emotional support.

Finally, I want to express my sincere gratitude to Universiti Tunku Abdul Rahman for providing me with a conducive environment and ample resources to complete my project.

DECLARATION

I hereby declare that the project report is based on my original work except for quotations and citations which have been duly acknowledged. I also declare that it has not been previously or concurrently submitted for any other degree at UTAR or other institutions.

(ONG KAI SIN)

APPROVAL SHEET

This project report entitled **"SYNTHESIS AND CHARACTERIZATION OF MICROWAVE ASSISTED ACETYLATED RICE STARCH / POLYETHYLENE OXIDE (PEO) BLENDS"** was prepared by **ONG KAI SIN** and submitted as partial fulfilment of the requirements for the degree of Bachelor of Science (Hons) Chemistry at Universiti Tunku Abdul Rahman.

Approved by:

S.M.Tan

(DR. TAN SHU MIN)
Supervisor
Department of Chemical Science
Faculty of Science
Universiti Tunku Abdul Rahman

Date: 13/09/2024

FACULTY OF SCIENCE

UNIVERSITI TUNKU ABDUL RAHMAN

Date: _____

PERMISSION SHEET

It is hereby certified that ONG KAI SIN (ID No: 20ADB02233) has completed this final year project entitled "**SYNTHESIS AND CHARACTERIZATION OF MICROWAVE ASSISTED ACETYLATED RICE STARCH / POLYETHYLENE OXIDE (PEO) BLENDS**" under the supervision of Dr. Tan Shu Min (Supervisor) from the Department of Chemical Science, Faculty of Science.

I hereby give permission to the Universiti to upload the softcopy of my final year project in pdf format into the UTAR Institutional Repository, which may be made accessible to the UTAR community and public.

Yours truly,

_____

(ONG KAI SIN)

Table of Contents

		Page
ABSTRACT		**ii**
ABSTRAK		**iv**
ACKNOWLEDGEMENT		**v**
DECLARATION		**vi**
APPROVAL SHEET		**vii**
PERMISSION SHEET		**viii**
TABLE OF CONTENTS		**ix**
LIST OF TABLES		**xiii**
LIST OF FIGURES		**xiv**
LIST OF ABBREVIATIONS		**xvii**
CHAPTER		
1	INTRODUCTION	1
2	LITERATURE REVIEW	6
	2.1 Polymer Blends	6

2.2 Starches 8

2.3 Starch Modifications 10

2.4 Poly(ethylene oxide) (PEO) 14

2.5 Isothermal crystallization of polymer 17

2.6 Melting behavior and miscibility of polymer blends 19

3 MATERIALS AND METHODS 21

3.1 Materials 21

3.2 Methods 22

3.2.1 Preparations of esterified rice starch 22

3.2.2 Attenuated Total Reflectance-Fourier Transform Infrared (ATR-FTIR) spectroscopy 23

3.2.3 Determination of degree of substitution 23

3.2.4 Preparation of PEO/ acetylated rice starch blend films 23

3.2.5 Differential Scanning Calorimetry (DSC) measurement 24

3.2.6 Analysis of isothermal crystallization behavior of pure PEO and PEO in PEO/acetylated rice starch blend 25

3.2.7 Study on melting behavior of pure PEO and PEO in PEO/acetylated rice starch blends 26

4 RESULTS AND DISCUSSION 28

4.1 Preparation of acetylated rice starch 28

4.1.1 Mechanism for acetylation of rice starch 28

4.1.2 Confirmation of the acetylated rice starch by Attenuated Total Reflectance-Fourier Transform Infrared (ATR-FTIR) spectroscopy 30

4.2 Determination of degree of substitution of acetylated rice starch 34

4.2.1 Effect of molar ratio of starch to acetic anhydride 35

4.2.2 Effect of amount of iodine 36

4.2.3 Effect of reaction time 37

4.3 Differential scanning calorimetry (DSC) measurements 38

4.3.1 Degree of crystallinity, X_c 39

4.3.2 Kinetics of Isothermal Crystallization 41

4.3.3 Estimation of equilibrium melting temperatures, T_m° of pure PEO and PEO in the blends 50

4.3.4 Determination of nucleation parameter, K_g for pure PEO and PEO/acetylated rice starch blend 54

4.3.5 Determination of the polymer-polymer interaction parameter, χ_{12} of PEO/acetylated starch blend 56

5 CONCLUSION 59

6	REFERENCES	62
7	APPENDIX A	74
8	APPENDIX B	76
9	APPENDIX C	78
10	APPENDIX D	82
11	APPENDIX E	83
12	APPENDIX F	84

LIST OF TABLES

Table		Page
3.1	List of chemicals and their respective suppliers.	21
4.1	Avrami parameters for PEO isothermal crystallization at different crystallization temperatures in a 90/10 PEO/acetylated starch blend.	45
4.2	Equilibrium melting temperatures, T_m°s, and stability parameters, $1/\gamma$ for various compositions of PEO/acetylated rice starch blends.	54
4.3	Nucleation parameters, K_g for pure PEO and different PEO/acetylated rice starch blends' compositions.	56

LIST OF FIGURES

Figure		Page
2.1	Molecular structure of amylose.	9
2.2	Molecular structure of amylopectin.	9
2.3	Chemical structure of PEO repeating unit.	14
3.1	Temperature program for isothermal crystallization for PEO/ acetylated starch blend.	26
3.2	Temperature program for studying the melting behavior of pure PEO and PEO/ acetylated rice starch blend at different Tc.	27
4.1	Reaction mechanism for iodine-catalysed acetylation of rice starch.	29
4.2	Reaction of sodium thiosulphate and iodine.	29
4.3	IR spectra of (a) native rice starch and (b) acetylated rice starch.	30
4.4	Infrared spectra of acetylated rice starch with various iodine amounts.	33
4.5	Free hydroxyl groups in anhydroglucose unit.	34

4.6	Degree of substitution versus molar ratio of rice starch to acetic anhydride at 0.25 mmol of iodine and reaction time of 2 minutes.	36
4.7	Degree of substitution versus amount of iodine at 1:3 starch to acetic anhydride ratio and reaction time of 2 minutes.	37
4.8	Degree of substitution versus reaction time at 1:3 starch to acetic anhydride ratio and 0.25 mmol iodine.	38
4.9	Degree of crystallinity, X_c of PEO versus weight fraction of acetylated starch at T_c = 40 °C.	40
4.10	DSC thermogram for 90/10 PEO/acetylated rice starch blend at T_c = 42.0 °C.	42
4.11	Avrami plots of 90/10 PEO/acetylated rice starch blend at T_cs of (●) 43.0 °C, (●) 44.0 °C, (●) 45.0 °C, (●) 46.0 °C and (●) 47.0 °C.	44
4.12	Half-time of crystallization, $t_{0.5}$ versus crystallization temperature, T_c for 70/30 PEO/acetylated rice starch blend.	46
4.13	Generalized rate constant, K_A^{1/n_A} versus crystallization temperature, T_c for 70/30 PEO/acetylated rice starch blend.	48
4.14	Graphs of (●) log (K_A^{1/n_A}) and (●) log ($t_{0.5}^{-1}$) versus crystallization temperature, T_c for 70/30 PEO/acetylated rice starch blend.	49

4.15 Reciprocal of half-time of crystallization, $t_{0.5}^{-1}$ versus weight fraction of acetylated starch for different ratios of PEO/acetylated rice starch blends at T_c s: (●) 40.0 °C, (●) 41.0 °C, (●) 42.0 °C, (●) 43.0 °C, (●) 44.0 °C. 50

4.16 Hoffman-Weeks plots for (●) pure PEO, (●) 80/20 and (●) 60/40 PEO/acetylated rice starch blends. 52

4.17 Graph of ln $t_{0.5}^{-1}$ versus $T_m^{\circ}/(T_c\Delta T)$ for pure PEO. 55

4.18 Plot of $\left(\frac{1}{T_m^o(PEO)} - \frac{1}{T_m^o(blend)}\right)$ against ϕ_2^2 for PEO/acetylated rice starch blends. 58

LIST OF ABBREVIATIONS

$1/\gamma$	Stability parameter
χ_{12}	Polymer-polymer interaction parameter
ϕ_1	Volume fraction of PEO
ϕ_2	Volume fraction of acetylated rice starch
ATR-FTIR	Attenuated Total Reflectance-Fourier Transform Infrared
DS	Degree of substitution
DSC	Differential scanning calorimetry
HCl	Hydrochloric acid
$\Delta H°$	Heat of fusion of perfectly crystalline PEO
ΔH_m	Melting enthalpy of PEO
IR	Infrared
ΔH°_m	Melting enthalpy of 100% crystalline PEO
K_A	Overall rate constant of crystallization
K_A^{1/n_A}	Generalized rate constant

K_g	Nucleation parameter
m_1	Degree of polymerization of PEO
m_2	Degree of polymerization of acetylated rice starch
n_A	Avrami exponent
NaOH	Sodium hydroxide
PEO	Poly(ethylene oxide)
r^2	Correlation coefficient
rpm	Revolution per minute
R	Universal gas constant
T	Time taken during the crystallization process
t_0	Induction period
$t_{0.5}$	Half-time of crystallization
$t_{0.5}^{-1}$	Reciprocal of half-time
ΔT	Undercooling
T_c	Crystallization temperature

T_m	Observed melting temperature
T_m°	Equilibrium melting temperature
V_0	Volume of HCl used for native rice starch
V_1	Volume of HCl used for acetylated rice starch
v_1	Molar volume of PCL
v_2	Molar volume of acetylated rice starch
w_{PEO}	Weight fraction of PEO
W	Mass of sample (native or acetylated rice starch)
X_c	Degree of crystallinity
X_t	Degree of conversion at time *t*

CHAPTER 1

INTRODUCTION

Polymers comprise numerous small molecules called monomers that are bonded together via covalent bonds to create long chains (Namazi, 2017). Polymers can be divided into two primary categories: synthetic polymers and natural polymers. A significant portion of packaging materials are derived from fossil hydrocarbons which are synthetic polymers, primarily single-use plastics, which make up over 50 % of the packaging industry (Surendren et al., 2022). The major fossil hydrocarbons used in single-use plastics for packaging include polyethylene, polypropylene, polyesters, polystyrene, polyvinyl chloride, and polyamides. These materials are favored because they are inexpensive, readily available, and possess excellent mechanical, barrier, and thermal properties. Most of these materials are non-degradable and non-recyclable, posing a significant environmental threat as they accumulate on land and in the ocean. It is estimated that a single plastic bag could take up to 1000 years to fully decompose (Li et al., 2022). In addition to impacting the global ecosystem, the production of synthetic polymers requires using fossil resources, which may eventually be depleted.

Natural polymers, on the other hand, originate from living organisms. This includes polysaccharides. Polysaccharides are widely used as packaging material for films and coatings because they offer an effective barrier against penetrants such as oxygen and carbon dioxide (Nešić et al., 2019). Starch and

cellulose are the most abundant polysaccharides found in nature and are extensively used in the production of biodegradable polymers for various functional applications. Starch is highly regarded as the premier alternative to petroleum-based single-use plastics due to its capability to form films, renewable nature, recyclability, and cost-effectiveness. Despite its advantages, starch does have some drawbacks, including low water resistance, weak mechanical properties, and the instability of starch-based plastics caused by variations in starch molecular structure and properties (Abe et al., 2021).

Modification of starch can be employed to enhance its properties and broaden its applications in the industrial sector. There are two methods of modifying starch: chemical modification and physical modification. One of the common chemical modifications is esterification to improve its hydrophobicity. This includes succinylation, acetylation, octenylsuccinic anhydride (OSA), and phosphorylation. Furthermore, starch can also undergo oxidation, acid hydrolysis, etherification, and crosslinking. The degree of substitution (DS) measures the extent of starch modification. DS refers to the average number of hydroxyl groups per repeating unit that have been replaced by a specific substituent (Liu et al., 2022).

Physical modifications of starches involve altering starch properties through physical treatments, without causing any chemical changes to the starch. Polymer blending is one of the physical modifications. It involves blending two

or more polymers, resulting in a new material with customized physical properties (Chandran, Shanks, and Thomas, 2014). The development of polymer blending results in the creation of new materials with improved properties. The products are made up of separate component polymers, each of which retains its mechanical properties with minimal or no loss. Starch blending aims to lower production expenses while enhancing barrier qualities and dimensional stability. The miscibility of the polymer blends significantly impacts its properties. Polymer blend miscibility can be categorized into three types: completely miscible (homogeneous), partially miscible, and completely immiscible (heterogeneous) (Parameswaranpillai, Thomas and Grohens, 2014). Additional physical modifications include pre-gelatinization, ultrasonication, heat-moisture treatment, and mechanical milling.

The classical pathway for polymer crystallization involves an initial nucleation step (primary nucleation) followed by a growth process (Xu, Reiter and Alamo, 2021). Nucleation mechanisms can be categorized into two types: primary nucleation and secondary nucleation. Primary nucleation happens in systems without crystals of the same crystallizing material and is further divided into two types: homogeneous and heterogeneous nucleation. If a solution lacks foreign particles or crystals of its type, a nucleus can only form through homogeneous nucleation. Heterogeneous nucleation occurs when foreign surfaces (particles) are present in the system, allowing nuclei to form on these surfaces at lower supersaturation levels compared to homogeneous nucleation.

Conversely, when nuclei are produced near crystals of the same material and function as attrition agents or seed crystals, this process is known as secondary nucleation (Hussein, 2022). Differential scanning calorimetry (DSC) is a widely used and convenient fundamental tool in the thermal analysis of polymers. DSC is capable of analyzing the crystallization and melting process of polymers under non-isothermal or isothermal conditions.

In this project, acetylation of rice starch was prepared by using acetic anhydride in the presence of iodine as a catalyst under microwave-assisted synthesis. The polymer blends of acetylated rice starch with poly(ethylene oxide) (PEO) were prepared using the solution casting method. The isothermal crystallization behavior of PEO in different blend compositions was investigated using DSC.

The objectives of this project are:

a) To modify rice starch via microwave assisted esterification using acetic anhydride in the presence of an iodine catalyst.

b) To confirm the incorporation of acetyl group into starch using Attenuated Total Reflectance-Fourier Transform Infrared (ATR-FTIR) spectroscopy.

c) To determine the degree of substitution (DS) of acetylated rice starch by back titration method.

d) To study the effect of the different ratios of rice starch to acetic anhydride, amount of iodine, and reaction time on the degree of substitution (DS) of the modified rice starch.

e) To prepare polymer blends of acetylated rice starch with PEO by solution casting method.

f) To investigate the isothermal crystallization behavior of PEO in PEO/acetylated rice starch blends.

g) To estimate the equilibrium melting temperature of PEO in PEO/acetylated rice starch blends.

h) To study the miscibility of PEO and acetylated rice starch based on Nishi-Wang equation.

CHAPTER 2

LITERATURE REVIEW

2.1 Polymer Blends

Polymer blending involves combining two or more polymers to create new materials with enhanced properties that surpass those of the individual components (Chandran, Shanks, and Thomas, 2014). The characteristics of polymer blends can be adjusted by varying the blend composition and mixing different polymers, depending on their intended application.

The final product's performance and properties depend on the blend components' miscibility, making the determination of polymer blend miscibility highly significant. The miscibility of the polymer blends will influence their mechanical properties, morphology, permeability, and degradation (Olabis, 2012). In a miscible blend, for example, homogeneity between the polymers is achieved, resulting in mechanical properties that are averaged between those of the individual components. Conversely, in immiscible blends, the polymers experience poor interfacial adhesion which leads to complete phase separation, thus resulting in polymer blends with inferior mechanical properties and varied microstructure (Panapitiya et al., 2016). Therefore, to achieve a blend with desired characteristics, it is essential to study the properties of the individual components of polymers and their miscibility when mixed.

Non-biodegradable plastics are a major concern due to their significant contribution to environmental pollution. Polymer blending has emerged as one of the most effective strategies to address the environmental issues related to plastic waste. The preparation of biodegradable polymer blends typically involves combining a thermoplastic resin with a biodegradable polymer (Samir et al., 2022). These blends are anticipated to be more biodegradable than traditional plastics. Starch is a biodegradable polymer. The blending of starch with synthetic polymers enhances their biodegradability, as starch naturally decomposes through microbial action, thus making it easier for natural processes like thermal oxidation and ultraviolet photo-degradation to break down the blend (Jayarathna, Andersson and Andersson, 2022). After the degradation process, the residual components are more environmentally friendly and do not contribute to environmental pollution. The biodegradation of low-density polyethylene/starch blends was studied by Abioye and Obuekwe (2020). The study's results demonstrated that biodegradable polymers can be created by blending low-density polyethylene with starch derived from Manihot esculenta, Zea mays, and Ipomoea batatas in various proportions. In addition, due to starch's inherent biodegradability, biodegradability improved as starch content increased in all the blend types.

Apart from resolving environmental issues, polymer blending is an appealing alternative offering several significant benefits, especially from an industrial standpoint. The benefits are that it can be used to create new materials

without the need for the synthesis of a novel polymer or copolymer, reducing the amount of time and money spent on research as well as the high cost of chemical synthesis and product development (Maha and Muhammed, 2023). Consequently, polymer blends are being recognized as a viable alternative to conventional plastics.

2.2 Starches

Starch is a biodegradable polymer that can be found in a variety of plant species. The purest form of starch consists of white granules that lack both odor and taste and are insoluble in cold water. This is known as native starch. Different plant species, influenced by geographical and climatic conditions, produce starch that varies in concentration, molecular size, and the structure of amylose and amylopectin. For instance, subtropical regions are used to grow corn, swampy areas to grow rice, tropical regions to grow cassava, and moderately cold climates to grow wheat or sweet potatoes (Kalia and Avérous, 2012). Moreover, starch polymer is the second most abundant biodegradable polymer in the world after cellulosic polymers.

Native starch is a semi-crystalline granule composed primarily of two types of glucan polymers which are amylose and amylopectin. The weight percentage of amylose and amylopectin in starch varies depending on the source, typically ranging from 20–25 % for amylose and 75–80 % for amylopectin

(Marichelvam, Jawaid and Asim, 2019). Amylose is composed of α-1,4-D-glucopyranosyl units arranged in linear or helical structures. In contrast, the amylopectin macromolecule contains α-D-glucopyranosyl units linked with α-1,6-glucosidic linkage approximately every 20 units, resulting in a highly branched, high molecular weight macromolecule (Atiwesh et al., 2021). The helical structure of the branch chains in amylopectin contributes to the crystalline regions of starch whereas amylose molecules are primarily located in the amorphous regions. The crystallinity of starch granules typically ranges from 15 % to 45 % (Singh et al., 2006). Figures 2.1 and 2.2 show the molecular structure of amylose and amylopectin respectively.

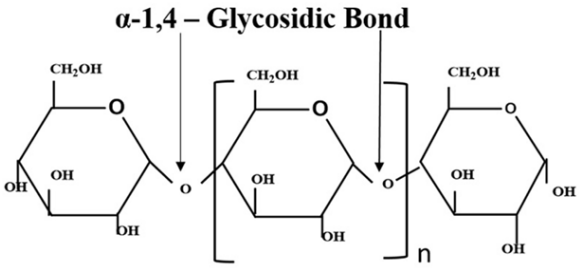

Figure 2.1: Molecular structure of amylose.

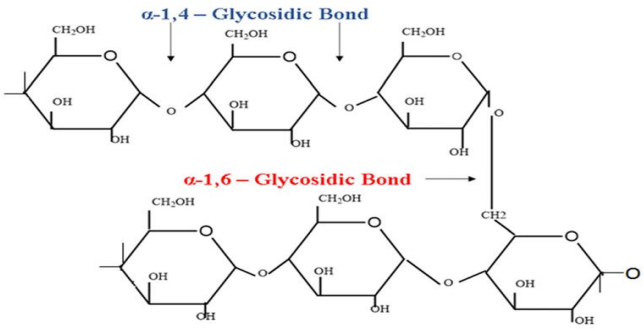

Figure 2.2: Molecular structure of amylopectin.

The amount of amylose within the starch granule greatly impacts its physical, chemical, and functional properties. The key factors influencing the morphology and functional properties of starch granules include the starch source, degree of polymerization, lipids, proteins, and inorganic components (Kalia and Avérous, 2012).

2.3 Starch Modifications

It is undeniable that starch has become highly desirable in the industry because of its plentiful availability, affordability, and capability to enhance a variety of products with its functional properties. Although starch has many appealing properties, several drawbacks restrict its commercial use. Starch-based films and coatings exhibit high water solubility and poor resistance to water. In addition, during melt processing, brittleness, retrogradation, and thermal degradation of starch can impact the films' mechanical integrity (Ogunsona, Ojogbo and Mekonnen, 2018).

Starch can be subjected to modification. Chemical, physical, and enzymatic modifications are the most widely used techniques for improving the properties of starch. Chemical modifications are still the most widely used method on an industrial scale since the reaction conditions can be easily modified to achieve the desired characteristics in the product. Besides that, due

to the possibility of increased functionality of the modified starch and the non-destructive nature of some of the processes compared to other modifications (Masina et al., 2017). Starch is susceptible to substitution reactions due to the presence of three hydroxyl groups in anhydroglucose unit. The starch's reactivity is also influenced by its grain size. The degree of susceptibility to modification increases with grain size. This is due to the fact that larger grains are easier for external factors to access (Bhatt et al., 2022). The degree of substitution (DS) can be used to determine the extent of modification. The average DS can range from 0 to 3 because each anhydroglucose unit contains three free hydroxyl groups.

One of the common chemical modifications is esterification. During starch esterification, hydroxyl groups are changed into hydrophobic groups. This increases swelling capacity, and hydrophobicity, and decreases the rate of retrogradation (Singh, Kaur, and McCarthy, 2007). Esterification occurs through the action of organic and inorganic acids, as well as their derivatives such as oxychlorides, acid anhydrides, and chlorides.

In a study conducted by Imre and Vilaplana (2020), various organic acid catalysts alongside monocarboxylic acid and anhydride reagents were employed to esterify corn starch. The successful acylation was shown in the IR spectrum by the appearance of some peaks: 1740 cm^{-1} (ester carbonyls), 1430 and 1370 cm^{-1} (alkyl $–CH_3$), and 1210 cm^{-1} (ester C–O stretch). Out of all the possible

organocatalysts that were tested (tartaric, citric, glycolic, L-lactic, L-malic, L-aspartic, and fumaric acids), only tartaric and citric acids demonstrated a significant catalytic effect, with DS values of 0.85 and 0.62, respectively. Tartaric acid was chosen to investigate the effects of different parameters including reaction temperature, catalyst concentration, and reaction time on the esterification of corn starch. The findings indicated that the DS increased when each of these factors increased. Moreover, when acetic anhydride was utilized as the reagent, the DS increased to a maximum of 2, much higher than the 0.15 and 0.05 found for propionic and butyric anhydrides. The reason for this was that the reactivity of anhydride decreased with increasing carbon chain length.

In addition, anhydride- and acid-type reagents in the acylation of starch were compared. It was discovered that anhydrides were a more effective reagent than carboxylic acids. In contrast to anhydrides, the molar mass of corn starch was significantly reduced by acid reagents because of the increased formation of water as a byproduct in substitution reactions with acids. The thermal stability of corn starch treated with acid was primarily influenced by its reduced molar mass and lower crystallinity. Anhydride-modified starch resulted in better thermal stability and decreased water sensitivity.

Another commonly employed modification is etherification. Etherified starch was found to have better rheological behavior and thermal stability characteristics (Compart et al., 2023). Epoxide reagents are typically used in the

etherification process of starch. Derina Paramitasari et al. (2024) conducted hydroxypropylation using a small amount of propylene oxide to enhance the sago starch's functional properties. The required molar substitution of 0.1 was attained with an optimized condition process that included 7 % wt. of propylene oxide, a pH of 11.92, and a reaction time of three hours. Because of the potential for side reactions, reaction times longer than three hours did not significantly increase the molar substitution as the amount of propylene oxide decreased after three hours. The resulting hydroxypropylated starch could withstand higher temperatures without changing the morphology and water-holding capacity, and swelling power can be enhanced.

Besides that, the impact of varying microwave powers (150-400 W) and durations (0-12 mins) on the DS of hydroxypropyl corn starch at 8 % propylene oxide was investigated by Lin et al. (2019). The microwave assisted method can significantly reduce the reaction time for hydroxypropyl starch compared to the traditional approach. It was observed that the DS of hydroxypropyl starch increased as the microwave power increased. Propylene oxide's interaction with available -OH of starch molecules was accelerated due to the microwave action exacerbating the thermal motion of the starch granules. However, the DS of hydroxypropyl starch did not increase as the microwave power increased. This was because, as the microwave power continued to increase, the temperature of the reaction system also rose. This led to localized gelatinization of starch granules, which hindered the reaction. Furthermore, as the microwave time

increased, the DS of hydroxypropyl starch initially increased and then began to decline. This was because starch molecules and propylene oxide have more time to react when microwave time increased. Nevertheless, prolonged microwave treatment can lead to an increase in the temperature of the reaction system, potentially causing local gelatinization and agglomeration of starch molecules which results in a decrease in DS.

2.4 Poly(ethylene oxide) (PEO)

Poly(ethylene oxide) (PEO) is a semi-crystalline, water-soluble thermoplastic polymer. PEO is available commercially in a broad range of molecular weights. The lower molecular weight with weights up to around 10,000 g/mol, are called poly(ethylene glycol)s (PEG). The higher molecular weights are referred to as PEO (Dimitrov and Tsvetanov, 2012). PEO is obtained by ring-opening polymerization of ethylene oxide under acid or basic catalysis. Figure 2.3 represents the structural unit of PEO.

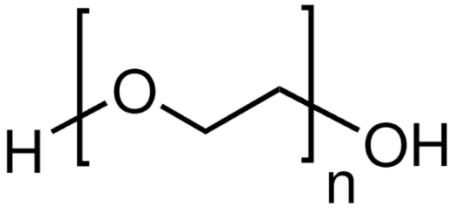

Figure 2.3: Chemical structure of PEO repeating unit.

Because of the hydroxyl group in PEO, it is highly hydrophilic and has low toxicity. As a result, PEO shows great promise for application in a variety of pharmaceutical and cosmetic products (Kai, Liow and Loh, 2014). However, the applicability of pure PEO films is restricted by their poor mechanical and physical properties (Amer Ali Mahdi et al., 2023). Consequently, blending PEO with other polymers is an effective method to create materials with improved properties.

Poly(ethylene oxide)-lignin blend for nanocellulose composites was studied by Tippabattini Jayaramudu et al (2019). Due to environmental concerns, industries have shown significant interest in composite materials made from renewable resources. Specifically, natural fiber-reinforced polymer (NFRP) composites, which are eco-friendly and low-cost, are widely used in the automotive and construction sectors. Lignin was utilized as the polymer matrix material; however, its brittleness, due to the globular structure of lignin fragments, led to unsatisfactory material properties for NFRP composites. The blending method can be employed to produce new materials with excellent performance.

The blending of PEO-lignin was utilized in the NFRP composite. The blends prepared showed the formation of intermolecular hydrogen bonds

between PEO and lignin. Besides that, differential scanning calorimetry (DSC) and thermogravimetric analysis (TGA) demonstrated strong miscibility between PEO and lignin. With increasing lignin content, the mechanical properties including Young's modulus and yield strength have improved. Additionally, the single lap joint tests conducted showed that the shear strength of the 30 % PEO-lignin blend was 189 % higher than that of pure PEO.

PEO was used as an electrolyte as it could dissolve lithium oxides and attain effective ionic conductivity at elevated temperatures (Xue, He, and Xie, 2015). However, it has the drawback of having low mechanical strength. Li et al. (2020) prepared a composite of high molecular weight PEO electrolytes by incorporating different wt% of MnO_2 nanosheets as filler. The highest mechanical performance was achieved at a concentration of 5 wt%, resulting in a maximum strength of approximately 2 MPa, nearly double that of pure PEO. The room conductivity also increased for the filled composite compared to the unfilled composite.

Another study was conducted by Kwon et al. (2022) to investigate the effect of PEO on mechanical, thermal, and degradation properties of poly (lactic acid) (PLA) with poly (butylene sebacate-co-terephthalate) (PBSeT) blends. PLA is a significant biodegradable plastic known for its unique properties. However, due to its poor degradation properties and low miscibility, it limits its application. The study showed that for PLA/PBSeT blends, PEO can function as

a compatibilizer and hydrolysis-accelerating agent. PEO-treated blends showed greater elongation at break, although their tensile strength was slightly decreased. Furthermore, DSC analysis indicated that with the addition of PEO has improved the miscibility of the blend.

2.5 Isothermal crystallization of polymer

Many researchers have extensively explored the kinetics of isothermal crystallization in polymer, using DSC as a valuable tool to monitor the crystallization process. The process of isothermal crystallization involves quenching the sample from its molten state to reach the crystallization temperature. The heat generated is then measured while the sample remains at a constant temperature (Foreman and Blaine, 1995).

Avrami's equation is widely utilized in examining the behavior of polymer crystallization in isothermal environments. The volume fraction of crystalline material as a function of time is expressed by this equation. The rate of nucleation and the volume increase in the lamellar crystals are two important kinetic events that are taken into account when deriving the Avrami equation (Chuah, Gan and Chee, 1999). The onset of crystallization is used as a reference zero time in isothermal crystallization (Kalkar and Deshpande, 2001). Nevertheless, there is a lag known as the induction period between the actual start of the nucleation process and the experimental zero-time reference.

Consequently, the Avrami exponent and rate constant values are inaccurate. The deviations become more apparent as the crystallization times increase. The Avrami model is still considered a reliable method for analyzing the kinetics of isothermal crystallization despite these flaws.

Amigo et al. (2019) studied the effect of starch nanoparticles (SNp) on the kinetics of isothermal crystallization of high-density polyethylene (HDPE). HDPE composites were prepared by in-situ polymerization using SNp with a diameter of around 70 nm. The Avrami plot of ln [-ln(1 – X_t)] versus ln (t – t_0) exhibited a linear relationship, suggesting that the isothermal crystallization behavior of the samples was adequately described by the Avrami equation. Avrami exponent n_A yielded qualitative details about the morphology of spherulite crystal growth and the nucleation mechanism. HDPE had an Avrami exponent of 1.7, indicating bidimensional structures. This exponent was unaffected by the presence of SNp, indicating that the nucleation mechanism of the HDPE matrix remained unchanged by these nanoparticles. Besides that, with an increase in the content of SNp, the crystallization half-time, $t_{0.5}$ decreased while the relative crystallinity increased, suggesting that starch nanocrystals functioned as nucleating agents to increase the rate of crystallization. This was because particles in the polymer melt can lower the energy needed to create a new surface and decrease the nucleus size necessary for crystal growth.

Tamaño-Machiavello et al. (2017) prepared poly(vinylidene fluoride) (PVDF)/ PEO polymer blend at 50/50 and 70/30 compositions to examine the

crystallization kinetics of PEO confined within semicrystalline PVDF. The blend films were produced by casting the solution at a temperature of 70 °C. For each polymer blend, the experimental results can be well-fitted to the Avrami equation at low conversion. At high conversion, deviations from linearity were observed, which were attributed to a change in the nucleation mechanism. In bulk PEO and the 50/50 sample, the maximum crystallinity attained during isothermal crystallization was roughly 70 %, whereas in the 70/30 blend, the fraction of PEO that can crystallize is only 5 % – 8 %. The crystallization rate increased for the 50/50 blend in comparison to bulk PEO due to PVDF's nucleating effect. However, the crystallization rate declined for the 70/30 sample. Therefore, it can be concluded that with more PVDF present, most PEO chains were unable to diffuse and integrate into the developing crystals due to the extreme confinement of PEO between PVDF crystallites.

2.6 Melting behavior and miscibility of polymer blends

The equilibrium melting temperature, T_m° is the melting point of crystals that have an extended chain structure and are in their most perfect state (Chung, Yeh and Hong, 2002). The equilibrium melting temperature, T_m°, is one of the most important parameters for characterizing a polymer.

Ding et al. (2020) conducted a study on the miscibility between purple sweet potato starches and wheat. The two semicrystalline polymers were blended with varying compositions of purple sweet potato starches containing

40 % and 60 % water content. The Hoffman–Weeks method was used to evaluate T_m°. The T_m° experienced a slight decrease as the amount of purple sweet potato starch increased. In addition, the values of T_m° with 60 % moisture content were lower compared to samples with 40 % moisture content. This showed that the amorphous segments were fully plasticized at high water content, resulting in the melting of crystals at low temperatures. Based on the Nishi Wang plot of $\left(\frac{1}{T_m^o(PEO)} - \frac{1}{T_m^o(blends)}\right)$ against ϕ_2^2, when the moisture content was 40 %, the value of $\left(\frac{1}{T_m^o(PEO)} - \frac{1}{T_m^o(blends)}\right)$ reduced more rapidly compared to 60 % moisture content, suggesting that the water content has an impact on the interaction of the binary system. The negative values of the interaction parameters for both moisture contents indicated that the wheat starch/purple sweet potato starch system was miscible.

Behera et al. (2020) investigated the melting behavior of poly(lactic acid) (PLA)/ PEO blend at a 70:30 weight ratio and the effect of the incorporation of carbon nanotube (CNT) on the melting behavior of the blend. It was found that the T_m° decreased for both individual PLA and PEO in the blends, indicating the polymers were miscible. The T_m° of PLA and PEO were slightly and marginally increased by a high loading of CNT, respectively. The rise in the T_m° value of PLA could be attributed to the reduction in entropy change caused by the finely dispersed CNT during melting.

CHAPTER 3

MATERIALS AND METHODS

3.1 Materials

A total of 9 chemicals used in the present study and their suppliers are tabulated in Table 3.1. Poly(ethylene oxide) (PEO) with an average molecular weight of 200,000 g/mol was used. All chemicals were used without further purification.

Table 3.1: List of chemicals and their respective suppliers.

Chemicals	Suppliers
Poly (ethylene oxide) (PEO)	Sigma-Aldrich
Rice starch	Sigma-Aldrich
Iodine	Fisher Scientific
Sodium thiosulphate	Uni-Chem
95 % ethanol	HmbG Chemicals
Sodium hydroxide	R&M Chemicals
Acetic anhydride	Merck Millipore
Hydrochloric acid	GENE Chemical
Chloroform	GENE Chemical

3.2 Methods

3.2.1 Preparations of esterified rice starch

Rice starch was esterified using acetic anhydride. Before being subjected to acetylation, any remaining water vapor was removed by drying rice starch in an oven at 55 °C for at least 24 hours. A 2.432 g (15 mmol) of starch was added with different molar ratios of starch to acetic anhydride (1:2, 1:3, 1:4, and 1:5) in a reactor vessel with a magnetic stir bar. Various amounts of iodine (0.05, 0.10, 0.25, 0.50, and 0.75 mmol) were added to the mixture. The mixture was stirred in a microwave synthesizer for two minutes. After that, the mixture was heated at 100 °C at 150 W for different reaction times (1, 2, 3, 4, and 5 minutes).

After heating, the mixture was transferred to a beaker and 2 mL of 2 M sodium thiosulphate was added to eliminate iodine and to end the reaction. A 40 mL of 95 % ethanol was added and the mixture was stirred for 15 minutes to precipitate out the acetylated rice starch. Vacuum filtration was used to filter the product and the product was rinsed with 95 % ethanol. Next, the product was dried in an oven at 55 °C for 48 hours. The dried product was sealed in the Ziploc bag and kept in a desiccator for further analysis.

3.2.2 Attenuated Total Reflectance-Fourier Transform Infrared (ATR-FTIR) spectroscopy

The Perkin-Elmer Spectrum Two FTIR Spectrometer with Universal ATR (Single Reflection Diamond) accessory was used to scan the wavenumber range between 4000 cm^{-1} to 400 cm^{-1} to obtain the IR spectra of both native and acetylated rice starch.

3.2.3 Determination of degree of substitution

A 0.5 g of acetylated rice starch and 20 mL of 75 % ethanol were mixed in an Erlenmeyer flask. The mixture was heated for 30 minutes in a water bath at 50 °C. After cooling to room temperature, 20 mL of a 0.5 M NaOH solution was added. An orbital shaker was used to shake the mixture for 24 hours at 60 rpm. Phenolphthalein was used as an indicator. The solution was then titrated with 0.5 M HCl until the solution color turned from pink color to colorless. The titration was repeated twice for both acetylated and native rice starch samples.

3.2.4 Preparation of PEO/ acetylated rice starch blend films

The blend films were prepared using the acetylated rice starch with the highest degree of substitution (DS). PEO/acetylated rice starch blends with varying compositions were prepared using the solution casting method in the

ratios of 100/0, 90/10, 80/20, 70/30, 60/40, and 50/50. Appropriate amounts of PEO and acetylated rice starch were dissolved in chloroform to form polymer solutions with a concentration of 3 % w/v. For instance, 0.90 g of PEO and 0.10 g of acetylated rice starch were mixed with 30 mL of chloroform to prepare a 90/10 blend. The solution was then heated in a water bath at 50 °C for 30 minutes to fully dissolve PEO and acetylated rice starch to form a homogenous mixture. The solution was subsequently poured onto a Petri dish, and the solvent was allowed to evaporate in an oven at 50 °C for 24 hours. Lastly, the blend films were stored in a desiccator until analysis.

3.2.5 Differential Scanning Calorimetry (DSC) measurement

The instrument utilized was a Mettler Toledo DSC 823 differential scanning calorimeter with an intra-cooler system. The calorimetric analysis by DSC were carried out under inert nitrogen gas at a flow rate of 20 ml/min to avoid any potential reaction of samples with the atmosphere. Every analysis was conducted using freshly prepared samples and aluminum crucibles containing sealed samples weighing 5.5 to 6.5 mg. The reference was an empty aluminum crucible.

3.2.6 Analysis of isothermal crystallization behavior of pure PEO and PEO in PEO/acetylated rice starch blend

At a constant heating rate of 20 °C/min, the sample was first heated from room temperature to the annealing temperature, T_a of 95 °C. The annealing temperature was held for three minutes to remove the sample's thermal history. After that, it was cooled to a specific crystallization temperature, T_c at a constant rate of -20 °C/min. The samples were maintained at T_c for a particular period of time, enabling them to crystallize under isothermal conditions until fully crystallized. The crystallization half-time, $t_{0.5}$, for various PEO/acetylated rice starch blend compositions was determined across the T_c range studied. Figure 3.1 represents the temperature program of isothermal crystallization of the polymer blends.

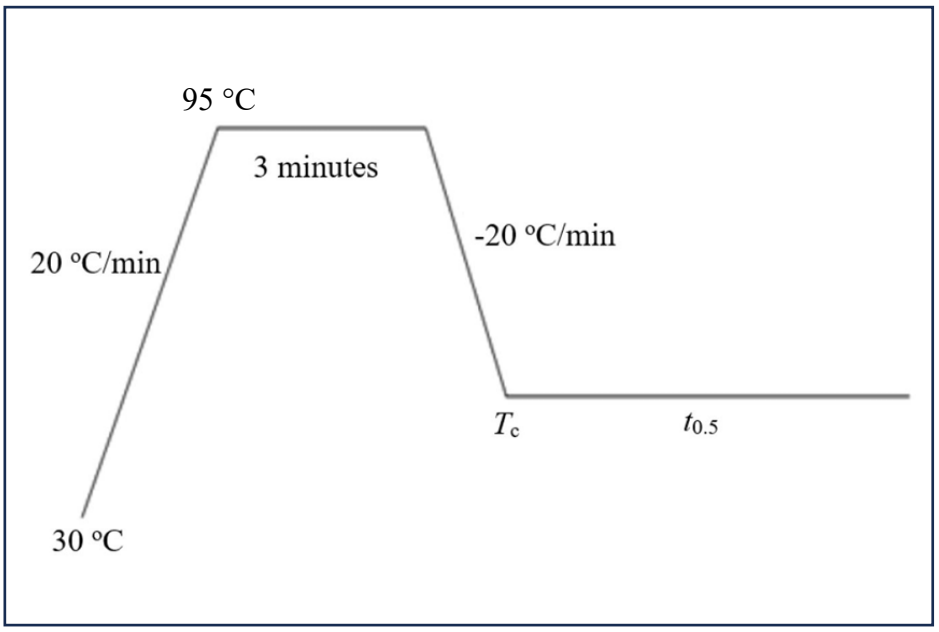

Figure 3.1: Temperature program for isothermal crystallization for PEO/ acetylated starch blends.

3.2.7 Study on melting behavior of pure PEO and PEO in PEO/acetylated rice starch blends

The melting temperature of pure PEO and PEO/acetylated rice starch blends was estimated by reheating the samples to 95 °C at a rate of 10 °C/min after they had undergone isothermal crystallization for five half-times ($5t_{0.5}$) at the specified T_c as shown in Figure 3.2. The first derivative curve's inflection point was used to determine the melting temperature, T_m.

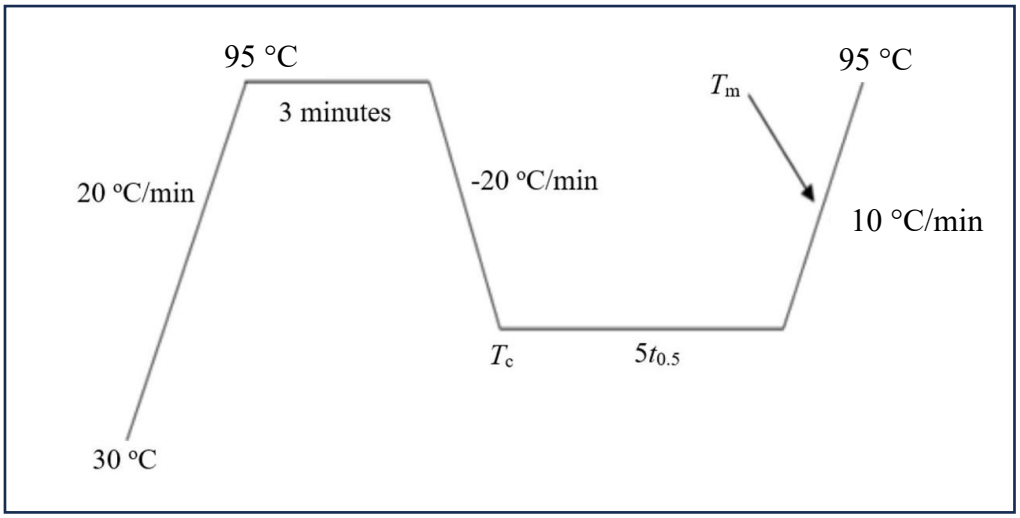

Figure 3.2: Temperature program for studying the melting behavior of pure PEO and PEO/ acetylated rice starch blend at different T_c.

CHAPTER 4

RESULTS AND DISCUSSION

4.1 Preparation of acetylated rice starch

4.1.1 Mechanism for acetylation of rice starch

Diop et al. (2011) proposed the mechanism for the acetylation of rice starch as shown in Figure 4.1. Iodine facilitated the first step in the reaction of acetic anhydride with hydroxyl groups by acting as a Lewis acid catalyst to activate the carbonyl carbon to let it more susceptible towards nucleophilic attack. The nucleophile: hydroxyl group (-OH) of rice starch will donate the lone pair electrons to the acyl group (C=O) of acetic anhydride (Li et al., 2009). After that, an acetic acid molecule was removed, and an iodine molecule was recreated to produce the ester product which was the acetylated rice starch. Since no solvent was needed for the acetylation of rice starch, the reaction can be classified as a green reaction.

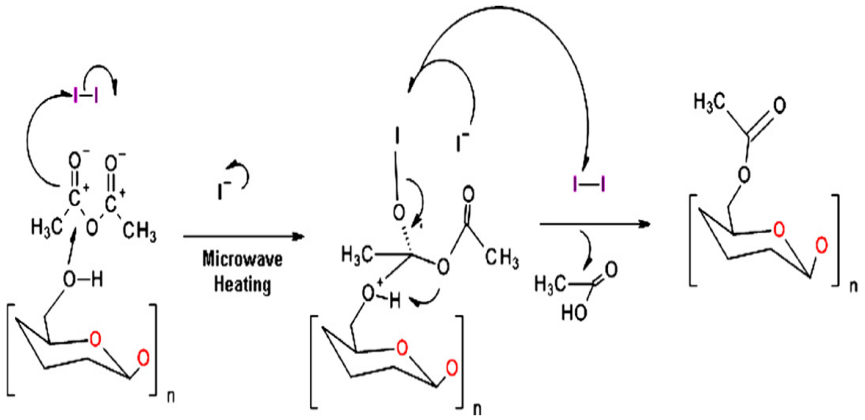

Figure 4.1: Reaction mechanism for iodine-catalyzed acetylation of rice starch.

The iodine catalyst can be easily removed after the acetylation reaction was completed, and the reaction can be stopped by converting the iodine to iodide with sodium thiosulphate (Diop et al., 2011). Figure 4.2 shows the chemical equation between sodium thiosulphate and iodine.

$$I_2 + 2S_2O_3^{2-} \rightarrow 2I^- + S_4O_6^{2-}$$

Figure 4.2: Reaction of sodium thiosulphate and iodine.

4.1.2 Confirmation of the acetylated rice starch by Attenuated Total Reflectance-Fourier Transform Infrared (ATR-FTIR) spectroscopy

ATR-FTIR spectroscopy was the most widely used technique to confirm the acetyl groups' incorporation into rice starch. Figure 4.3 illustrates the IR spectra of native and esterified rice starch.

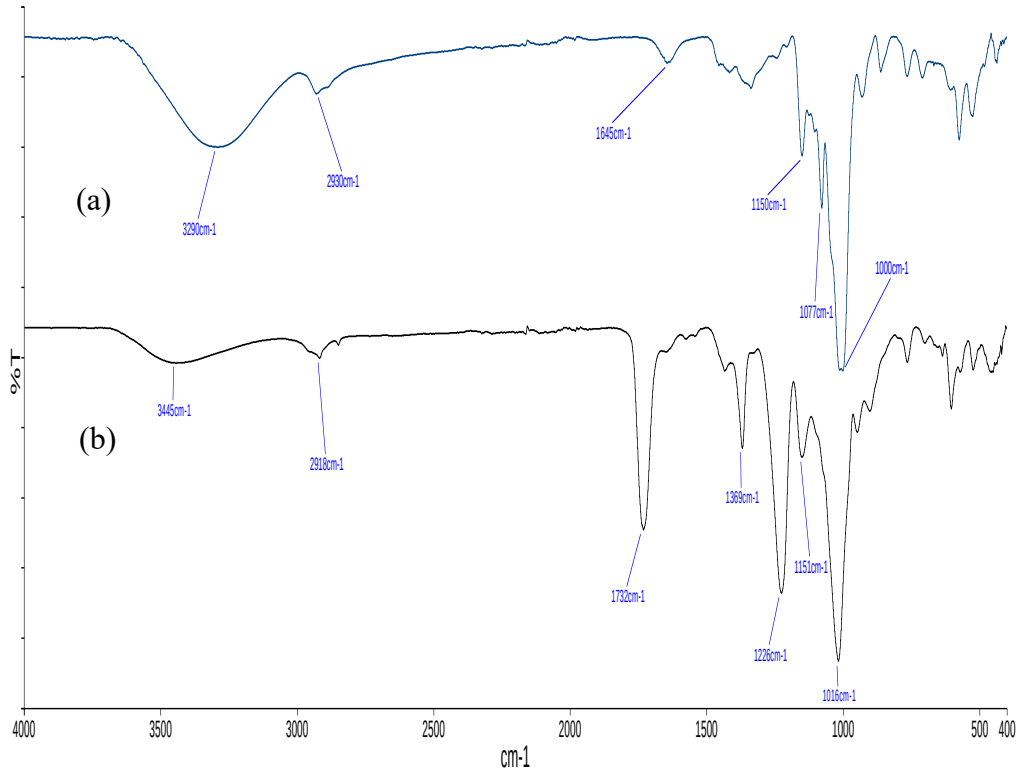

Figure 4.3. IR spectra of (a) native rice starch and (b) acetylated rice starch.

Figure 4.3 (a) indicates the IR spectra for native rice starch. There was a significant broad peak at 3290 cm^{-1} representing the hydroxyl group (-OH) stretching vibration. Besides, the peak at 2930 cm^{-1} was assigned to the aliphatic C-H stretching vibration. Another peak at 1645 cm^{-1} was attributed to the adsorbed water. Next, the peaks at 1150 cm^{-1}, 1077 cm^{-1}, and 1000 cm^{-1} indicated the stretching vibration of the C-O bond.

Successful acetylation of rice starch was verified by the appearance of some new peaks as shown in Figure 4.3 (b). three evident peaks at 1732 cm^{-1}, 1369 cm^{-1}, and 1226 cm^{-1} represented the stretching vibration of the ester carbonyl group (C=O), symmetry deformation vibration of CH_3, and the stretching vibration of C-O in the acetyl group respectively (Chi et al., 2008). The product was presumed to be free of unreacted acetic anhydride as there was no peak in the range of 1850 cm^{-1} – 1760 cm^{-1}, and it was free from acetic acid byproduct because there was no peak in the region of 1700 cm^{-1}. The successful acetylation of rice starch can be further proven by the decrease in the intensity of the hydroxyl group peak and the increase in the intensity of the carbonyl group peak (Biswas et al., 2007). This was because the acetyl group of the acetic anhydride replaced the hydroxyl group of the native starch.

The infrared spectra of acetylated rice starch with various iodine amounts are displayed in Figure 4.4. The intensity of the carbonyl stretching vibration at 1732 cm^{-1} was found to increase with an increase in iodine

concentration up to 0.25 mmol, suggesting that the rate of acetylation increased with iodine concentration up to 0.25 mmol. Nevertheless, the increase in the intensity of the -OH at 3418 cm^{-1} may be due to the presence of water molecules.

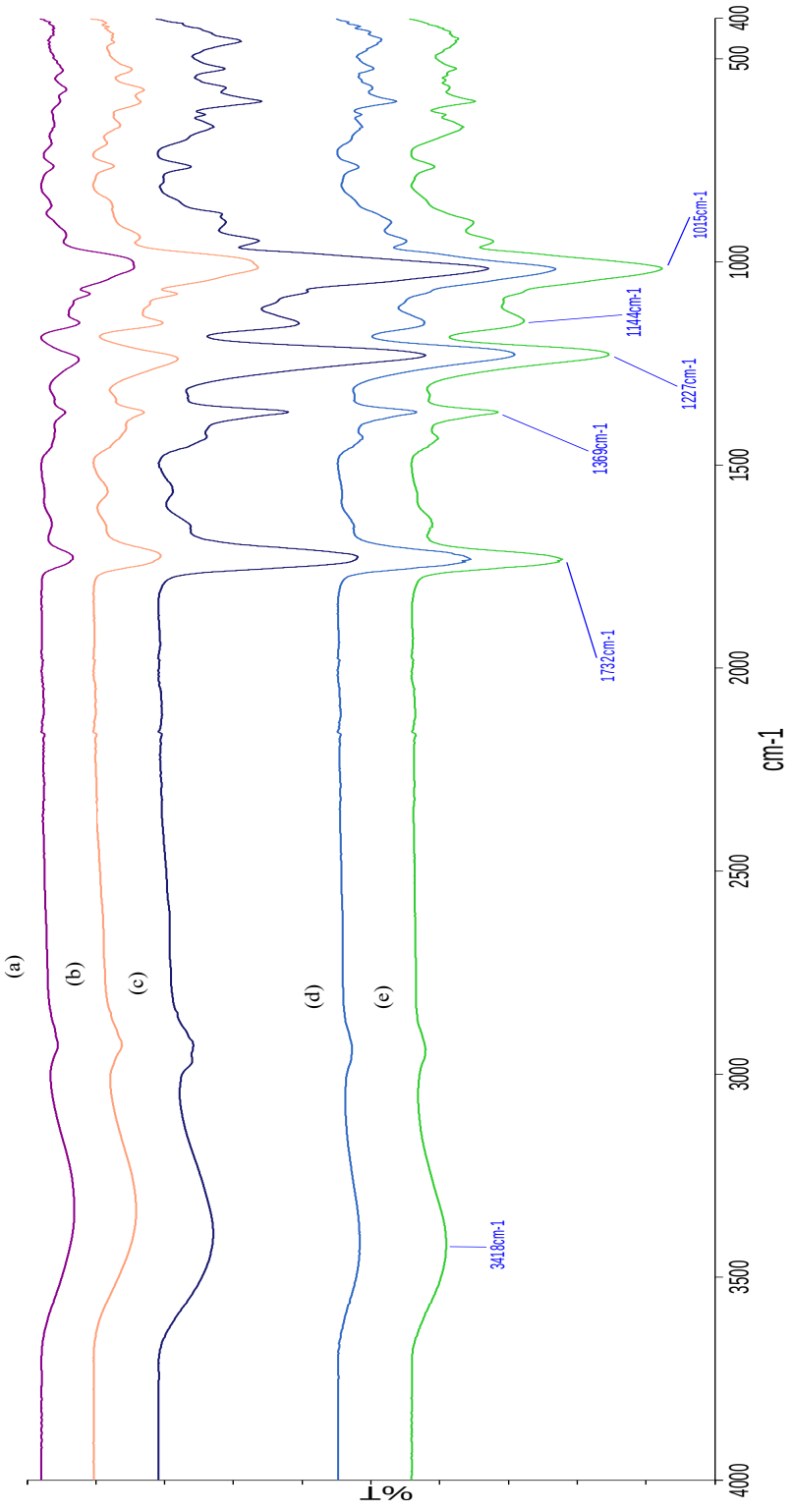

Figure 4.4: Infrared spectra of acetylated rice starch with various iodine amounts (a) 0.05 mmol, (b) 0.10 mmol, (c) 0.25 mmol, (d) 0.50 mmol, and (e) 0.75mmol.

4.2 Determination of degree of substitution of acetylated rice starch

The back titration method was used to examine the effects of the molar ratio of starch to acetic anhydride, the amount of iodine, and the reaction time on the degree of substitution (DS) of acetylated rice starch. The maximum DS is 3 as there are 3 free hydroxyl groups located at the C2, C3, and C6 carbon susceptible to nucleophile attack (Lewicka, Siemon and Kurcok, 2015).

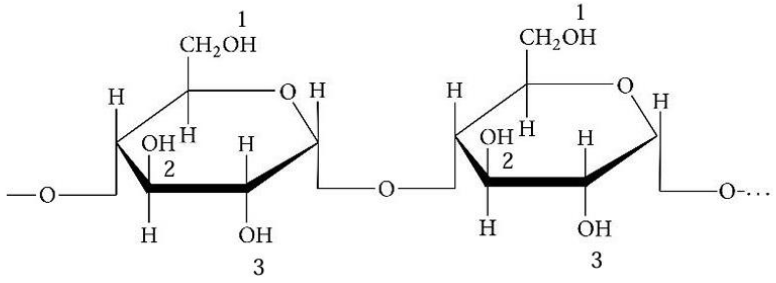

Figure 4.5: Free hydroxyl groups in anhydroglucose unit.

The DS can be calculated using the Equation 4.1 provided by Diop et al. (2011).

$$\% \text{ Acetyl group} = \frac{(V_0 - V_1)}{W} \times M \times 0.043 \times 100\% \qquad \text{(Equation 4.1)}$$

V_0 and V_1 are the volumes of HCl needed in milliliters for native starch and acetylated rice starch to turn the solution color from pink to colorless during

back titration. *W* is the mass of the acetylated rice starch in grams. *M* is the concentration of HCl used.

The DS can then be determined by substituting the calculated percentage of the acetyl group into Equation 4.2, where 43 and 162 are the molecular weight of the acetyl group and the anhydroglucose unit in starch respectively.

$$\text{Degree of substitution} = \frac{162 \times \%\ \text{Acetyl group}}{4300 - (42 \times \%\ \text{acetyl group})} \qquad \text{(Equation 4.2)}$$

4.2.1 Effect of molar ratio of starch to acetic anhydride

From the graph DS against the molar ratio of starch to acetic anhydride as shown in Figure 4.6, when the ratio of starch to acetic anhydride increased, the DS of the rice starch was observed to rise as well, reaching a maximum at a ratio of 1:4 molar ratio. This increase can be attributed to the fact that more molecules of acetic anhydride are available to collide with starch molecules, thus increased the rate of reaction (Xu, Vesselin Miladinov, and Hanna, 2004). However, the DS decreased after a 1:4 molar ratio. This occurred because the solution became more acidic as acetic anhydride concentration increased. When the acidity increased, the rate at which ester bonds hydrolyzed outpaced the rate

at which they formed, thus decreased the acetylation of starch (Biswas et al., 2009).

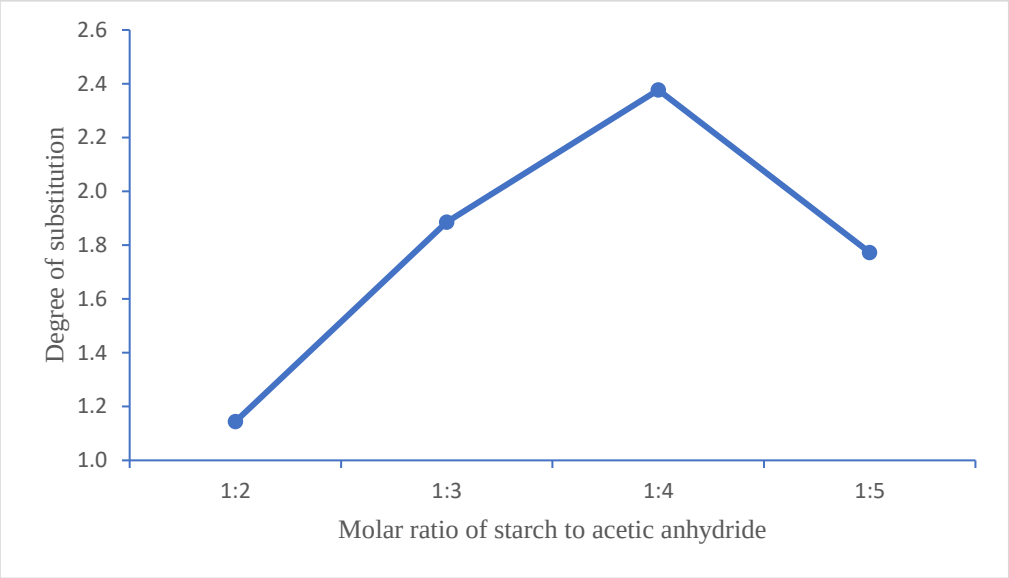

Figure 4.6: Degree of substitution versus molar ratio of rice starch to acetic anhydride at 0.25 mmol of iodine and reaction time of two minutes.

4.2.2 Effect of amount of iodine

Figure 4.7 shows the graph of DS against the amount of iodine. When the amount of iodine increased, it was found that the DS of the rice starch increased until reaching a maximum at 0.25 mmol of iodine. This was attributed to the fact that iodine functioned as a catalyst, offering a different reaction pathway with a lower activation energy, thus accelerating the acetylation reaction. The iodine facilitated the process by activating the carbonyl group of the acetic anhydride, thereby promoting the nucleophilic attack by the hydroxyl

groups in the starch (Diop et al., 2011). Nevertheless, as the iodine concentration increased above 0.25 mmol, the excess iodine started to react with the acetic acid to form iodidric acid, which caused the DS to drop (Ramírez-Arreola et al., 2009). As a result, the rate of acetylation was inhibited and the DS was lowered.

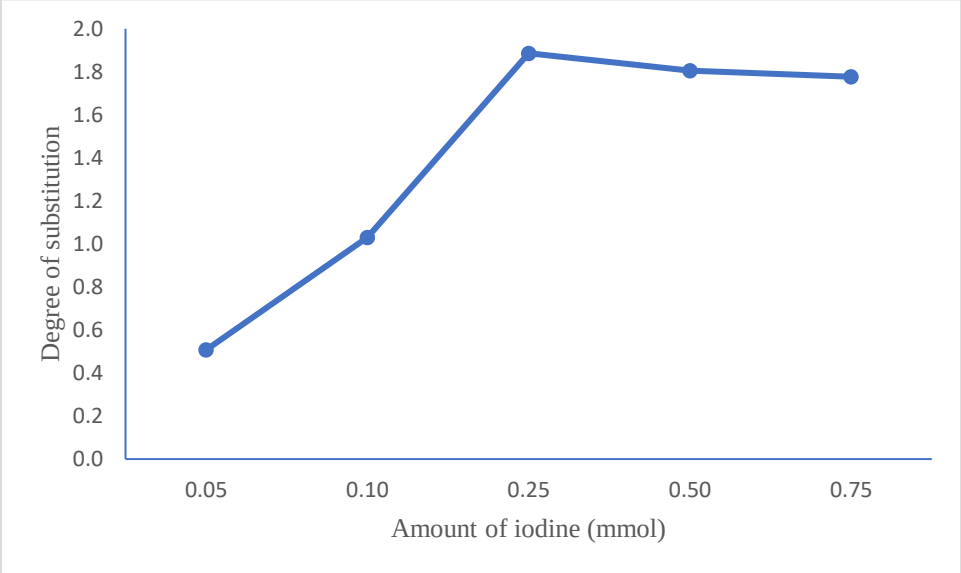

Figure 4.7: Degree of substitution versus amount of iodine at 1:3 rice starch to acetic anhydride molar ratio and reaction time of two minutes.

4.2.3 Effect of reaction time

The graph of DS versus reaction time is displayed in Figure 4.8. It was observed that the DS increased when reaction time increased up to two minutes. This could be explained by the fact that as reaction time increased, more microwave energy was available, leading to the formation of more reaction sites. Besides, acetyl groups have more time to diffuse and adsorb onto the starch

molecules to let the reaction occur. However, as the reaction time increased further, the DS then dropped due to the gradual consumption of acetic anhydride and the hydrolytic of acetylated rice starch occurred more quickly than the formation of acetylated rice starch (Zhang et al., 2013). Another reason was that extended microwave treatment may raise the temperature of the reaction system, which could result in localized gelatinization and clumping of starch molecules (Lin et al., 2019).

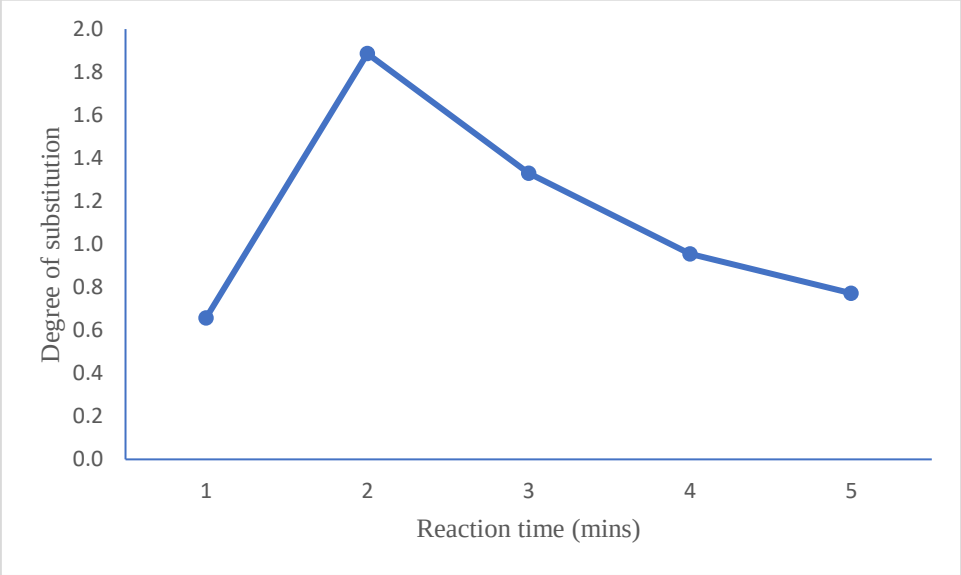

Figure 4.8: Degree of substitution versus reaction time at 1:3 rice starch to acetic anhydride molar ratio and 0.25 mmol iodine.

4.3 Differential scanning calorimetry (DSC) measurements

The thermoanalytical method known as differential scanning calorimetry (DSC) operates based on the heat flow principle. This method involves

measuring the difference in heat flow between the sample and a reference as they are exposed to a controlled temperature program (Höhne, Hemminger, and Flammersheim, 2013). DSC is frequently used to study transitions such as melting, glass transitions, and crystallization.

4.3.1 Degree of crystallinity, X_c

Polymers in solid form consist of two primary regions: the structured crystalline region and the unstructured amorphous region. The proportion of crystalline to amorphous regions differs from one polymer to another. DSC is commonly used to measure the heat released during the melting (fusion) of polymers, a process that reveals the polymers' degree of crystallinity, X_c (Crompton, 2006). The value of X_c is calculated by dividing the melting enthalpy of the polymer by the melting enthalpy of a completely crystalline pure polymer. The calculation also considers the amount of polymer to assess its impact on the crystallinity. Using Equation 4.3, the X_c of PEO in the blends can be determined (Kong and Hay, 2002).

$$X_c = \frac{\Delta H_m}{\Delta H_m^0 \times w_{PEO}} \text{ x } 100\% \qquad \text{(Equation 4.3)}$$

where ΔH_m and ΔH°_m are the melting enthalpies of the PEO in the blends and 100 % crystalline of PEO, and w_{PEO} is the weight fraction of PEO in the

PEO/acetylated rice starch blends. ΔH°_{m} was obtained from the literature to be 196.6 J/g (Araneda et al., 2011). In Figure 4.9, the X_c of PEO is plotted against the weight fraction of acetylated rice starch at a temperature of T_c = 40.0 °C. The estimated X_c of pure PEO was 63.2 %.

As the amount of acetylated rice starch increased, it was observed that the overall degree of crystallinity of PEO decreased. Chain mobility provides an explanation for this trend. One of the main factors in polymer crystallization is sufficient chain mobility. Acetylated starch is comparatively more amorphous than PEO. According to Li (1985), amorphous components caused blends to become more viscous, which prevents chains from moving freely. Consequently, the X_c decreased. As the amount of acetylated rice starch in the blend increased, the amorphous component diluted the crystalline PEO component, resulting in a significant decrease in PEO nucleation and crystal growth (Rohindra and Khurma, 2007).

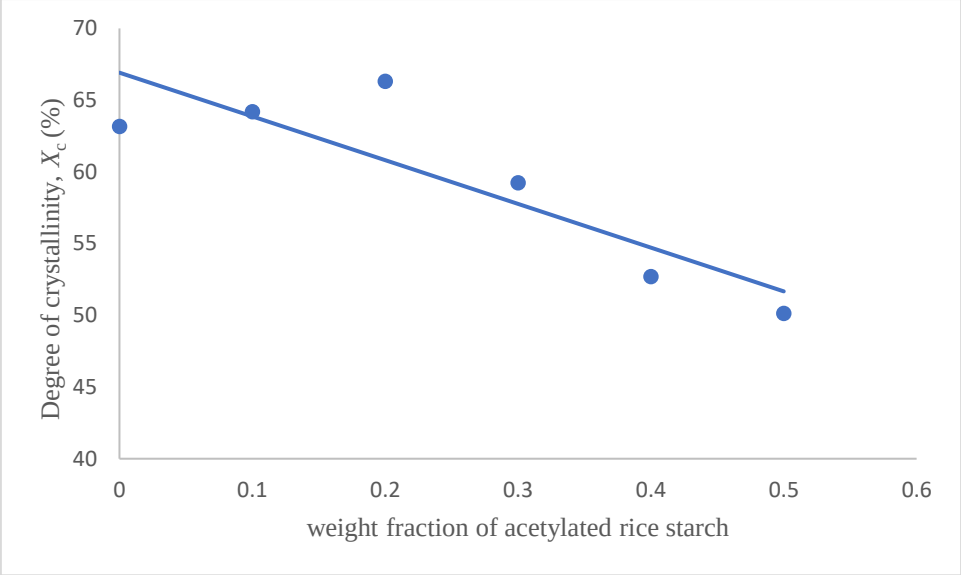

Figure 4.9: Degree of crystallinity, X_c of PEO versus weight fraction of acetylated rice starch at T_c = 40 °C.

4.3.2 Kinetics of Isothermal Crystallization

DSC was used to examine the isothermal crystallization behavior of PEO in the PEO/acetylated rice starch blends at different crystallization temperatures. A DSC thermogram with a crystallization exotherm for a blend of 90/10 PEO and acetylated rice starch at T_c = 42.0 °C is shown in Figure 4.10. The induction period, t_0, for crystallization, is shown in Figure 4.10, was defined as the time at which the crystallized mass started to increase markedly. The degree of conversion, X_t, can be described using the area under the exothermic peak. The amount of heat released can be obtained by integrating the peak area. Equation 4.4 is used to calculate X_t:

$$X_t = \frac{\Delta H_t}{\Delta H_\infty} = \frac{\int_0^t \left(\frac{dH}{dt}\right) dt}{\int_0^\infty \left(\frac{dH}{dt}\right) dt} = \frac{a_t}{a_\infty} \qquad \text{(Equation 4.4)}$$

ΔH_t and ΔH_∞ represent the heat released at time t and at infinite time, respectively; (dH/dt) is the sample's heat flow rate; a_t and a_∞ denote the area under the exothermic peak at time t and as t approaches infinity, respectively. The X_t can thus be determined as the ratio of the peak area at time t to the peak area at t approaching infinity.

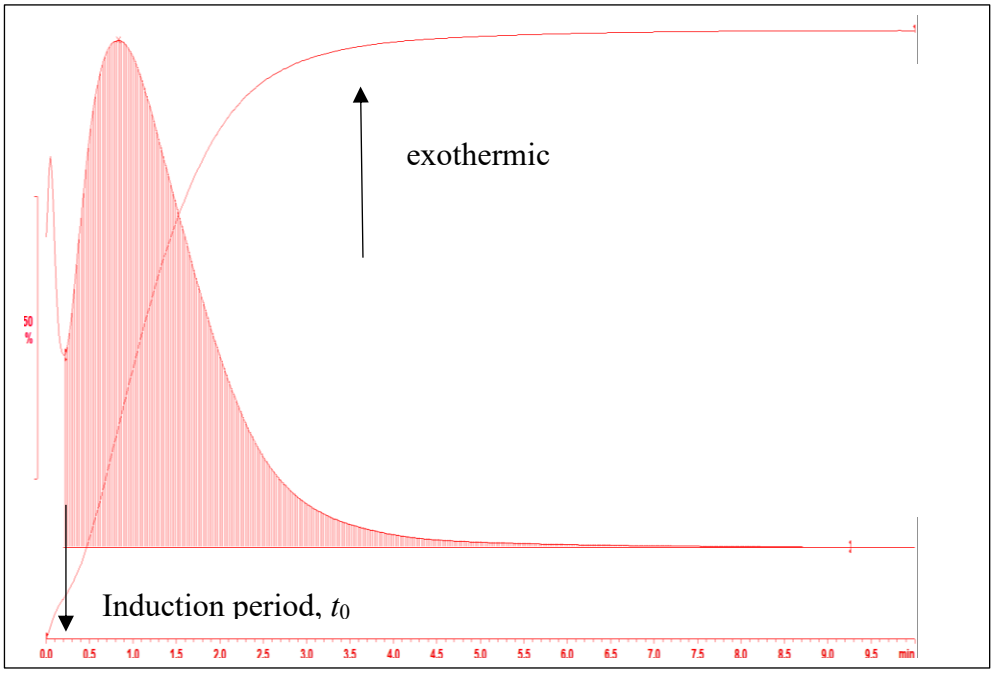

Figure 4.10: DSC thermogram for 90/10 PEO/acetylated rice starch blend at T_c = 42.0 °C.

The kinetics of PEO's isothermal crystallization in the PEO/acetylated rice starch blends were analyzed using the Avrami equation. The Equation 4.5 illustrates the widely recognized Avrami equation (Avrami, 1939):

$$1 - X_t = \exp[-K_A(t - t_0)^{nA}] \qquad \text{(Equation 4.5)}$$

X_t denotes the degree of conversion at time t; K_A is the overall crystallization rate constant, a kinetic parameter influenced by the holding temperature, nucleation rate, and growth rate; t is the time elapsed during the crystallization process; t_0 is the induction period; and n_A is the Avrami exponent, which indicates the nucleation rate and growth morphology. By applying logarithms to both sides of Equation 4.5, a linearized Avrami equation is derived as shown in Equation 4.6:

$$\log[-\ln(1 - X_t)] = \log K_A + n_A \log(t - t_0) \qquad \text{(Equation 4.6)}$$

From the Avrami plot of log[-ln(1 – X_t)] versus log(t – t_0), a linear line with a positive slope of n_A and an intercept of log K_A can be obtained. Figure 4.11 displays Avrami plots for PEO in a 90/10 PEO/acetylated starch blend at different crystallization temperatures.

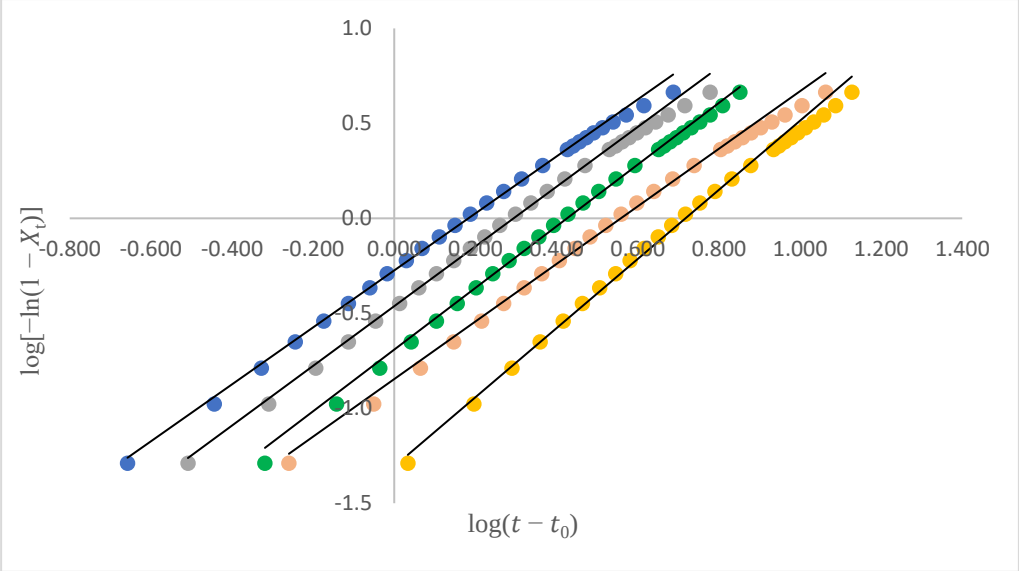

Figure 4.11: Avrami plots of 90/10 PEO/acetylated rice starch blend at T_cs of (●) 43.0 °C, (●) 44.0 °C, (●) 45.0 °C, (●) 46.0 °C and (●) 47.0 °C.

From Figure 4.11, the experimental data could be fitted into the Avrami equation at different crystallization temperatures with a degree of conversion of up to 95 %. However, once the degree of conversion reached 95 %, deviation from the straight line started to happen. Typically, the two stages of the crystallization process are known as primary and secondary crystallization, respectively. Primary crystallization, which followed the linear section of the Avrami plot, is the formation of crystal nuclei from the polymer melt. On the other hand, the formation of nuclei in the presence of pre-existing crystals is known as secondary crystallization. In secondary crystallization, crystals grow unhindered until they begin to collide with one another. This collision process, referred as crystal impingement, disrupts the further crystal nucleation (Thakur and Kessler, 2015). This consequently caused the resulting Avrami exponent to decrease, producing a non-linear Avrami plot.

The values of Avrami parameters for the isothermal crystallization of PEO in the 90/10 PEO/acetylated starch blend are tabulated in Table 4.1. The combination of thermal and athermal nucleation mechanisms was indicated by the non-integral values of the Avrami exponent, n_A (Kalkar, Deshpande and Kulkarni, 2008). The Avrami exponent, n_A determined for PEO in 90/10 PEO/acetylated rice starch blend, which ranged from 1.50 to 1.82 suggested a two-dimensional crystal growth geometry for PEO in the blends. The nucleation mechanism of PEO remained unchanged upon the addition of acetylated rice starch, as evidenced by the values of the Avrami exponent, n_A, of pure PEO also fell in this range for the whole crystallization temperature. The other blend compositions studied showed similar trends.

Table 4.1: Avrami parameters for PEO isothermal crystallization at different crystallization temperatures in a 90/10 PEO/acetylated starch blend.

Crystallization temperature, T_c (°C)	Avrami exponent, n_A	Generalized rate constant, K_A^{1/n_A}	Half-time of crystallisation, $t_{0.5}$ (min)	Correlation coefficient, r^2
43	1.50	0.66	1.17	0.999
44	1.57	0.51	1.54	0.999
45	1.62	0.37	2.09	0.998
46	1.51	0.28	2.79	0.997

47	1.82	0.19	4.13	0.997

The half-time of crystallization, $t_{0.5}$ is the duration needed to achieve 50 % of total crystallization. After the induction period, t_0, the area under the crystallization peak was used to calculate values of $t_{0.5}$. A plot of $t_{0.5}$ against T_c is shown in Figure 4.12. With increasing T_c, it can be seen that $t_{0.5}$ increased exponentially which means that the crystallization rate decreased exponentially with a higher crystallization temperature.

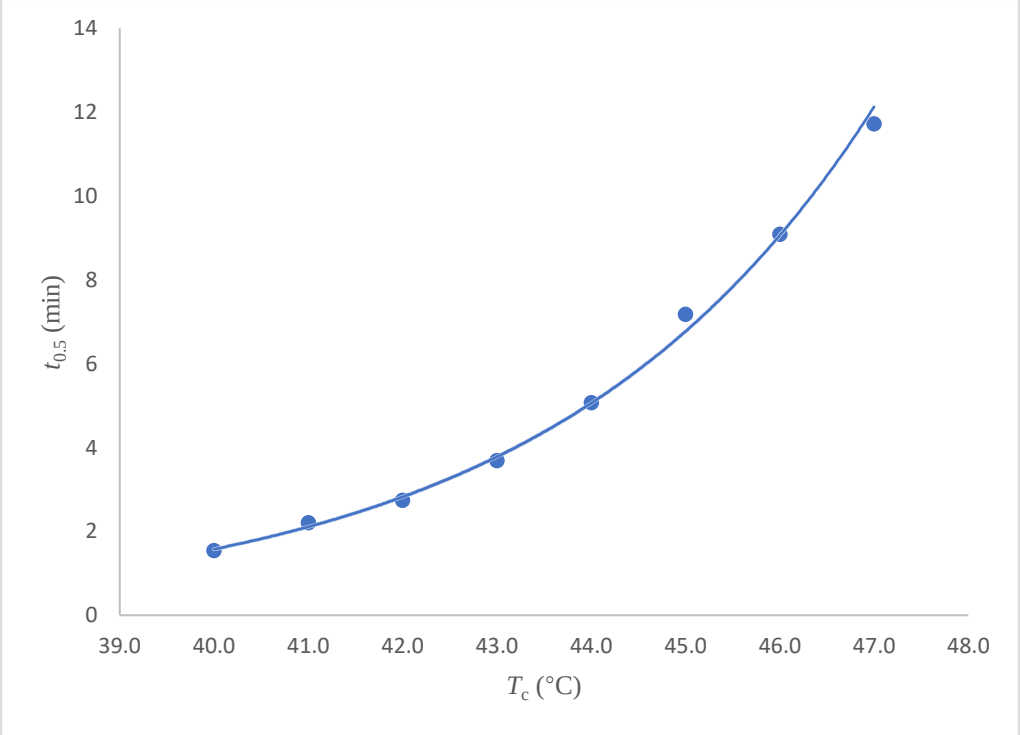

Figure 4.12: Half-time of crystallization, $t_{0.5}$ versus crystallization temperature, T_c for 70/30 PEO/acetylated rice starch blend.

This phenomenon can be explained by two opposing processes: nucleation and molecular transport (diffusion) in the polymer melt. At high

crystallization temperatures, the diffusion rate increased due to high thermal energy. The polymer's chain mobility was so high in these conditions that the crystallization process was prevented. The nucleation rate was extremely low in this instance (Pereira et al., 2010). Consequently, the process of crystallization was slowed down. The same trend was obtained across all the blend compositions studied.

In addition to the crystallization half-time, the generalized rate constant, K_A^{1/n_A}, can also be used to express the crystallization rate. Both the Avrami exponent, n_A, and the overall rate constant of crystallization, K_A, were used to calculate the values of K_A^{1/n_A}. Graph of K_A^{1/n_A} versus T_c for a 70/30 blend of PEO/acetylated rice starch is illustrated in Figure 4.13. The generalized rate constant, K_A^{1/n_A}, was found to decrease exponentially with increasing crystallization temperature, T_c. This suggested that the crystallization rate decreased exponentially as the crystallization temperature increased. The same trend was obtained across all the blend compositions studied.

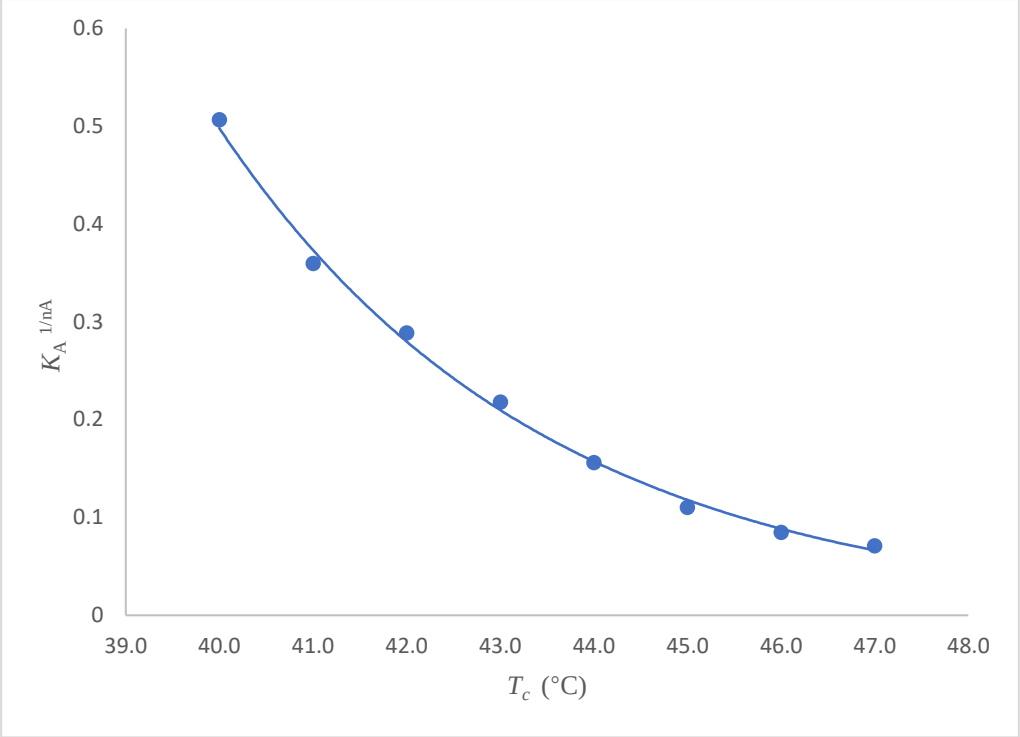

Figure 4.13: Generalized rate constant, K_A^{1/n_A} versus crystallization temperature, T_c for 70/30 PEO/acetylated rice starch blend.

Equation 4.7 established a relationship between the generalized rate constant, K_A^{1/n_A}, and the reciprocal of the crystallization half-time, $t_{0.5}^{-1}$ (Qiu et al., 2005).

$$t_{0.5}^{-1} = \left(\frac{K_A}{\ln 2}\right)^{1/n_A} \qquad \text{(Equation 4.7)}$$

Figure 4.14 depicts two logarithmic plots: one showing the generalized rate constant, K_A^{1/n_A}, against crystallization temperature, T_c, and the other showing the reciprocal of the crystallization half-time, $t_{0.5}^{-1}$, against crystallization temperature, T_c. Both plots reveal a linear relationship where log

($t_{0.5}^{-1}$) and log (K_A^{1/n_A}) decreased as the crystallization temperature increased. Given that both plots showed the same trend, it can be said that as the crystallization temperature, increased, the crystallization rate decreased as well. The same trend was obtained across all the blend compositions studied.

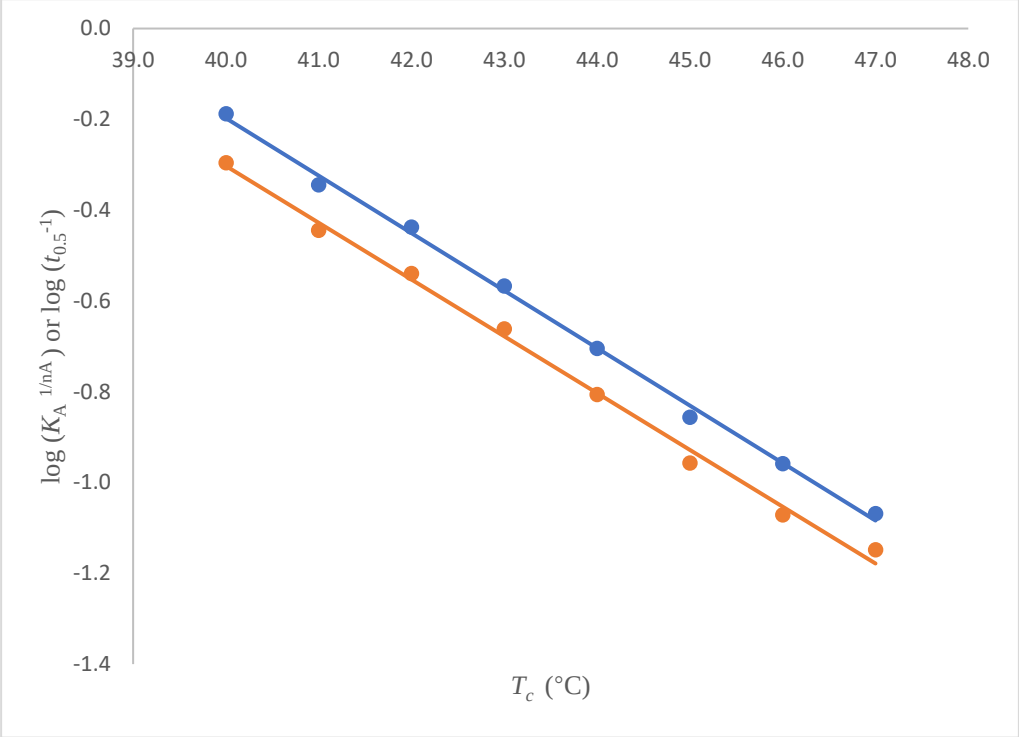

Figure 4.14: Graphs of (●) log (K_A^{1/n_A}) and (●) log ($t_{0.5}^{-1}$) versus crystallization temperature, T_c for 70/30 PEO/acetylated rice starch blend.

Based on Figure 4.15, it was observed that the crystallization rate of PEO in the PEO/acetylated starch blend decreased with increasing acetylated starch content. This was due to the addition of starch increased the activation energy required for crystallization (Liu, Wang, and Sun, 2004). This phenomenon could also be explained by considering chain mobility. At higher starch concentrations, the blend's viscosity increased due to the aggregation of starch granules. This

led to reduced chain mobility of PEO within the blend, which in turn hindered crystal growth.

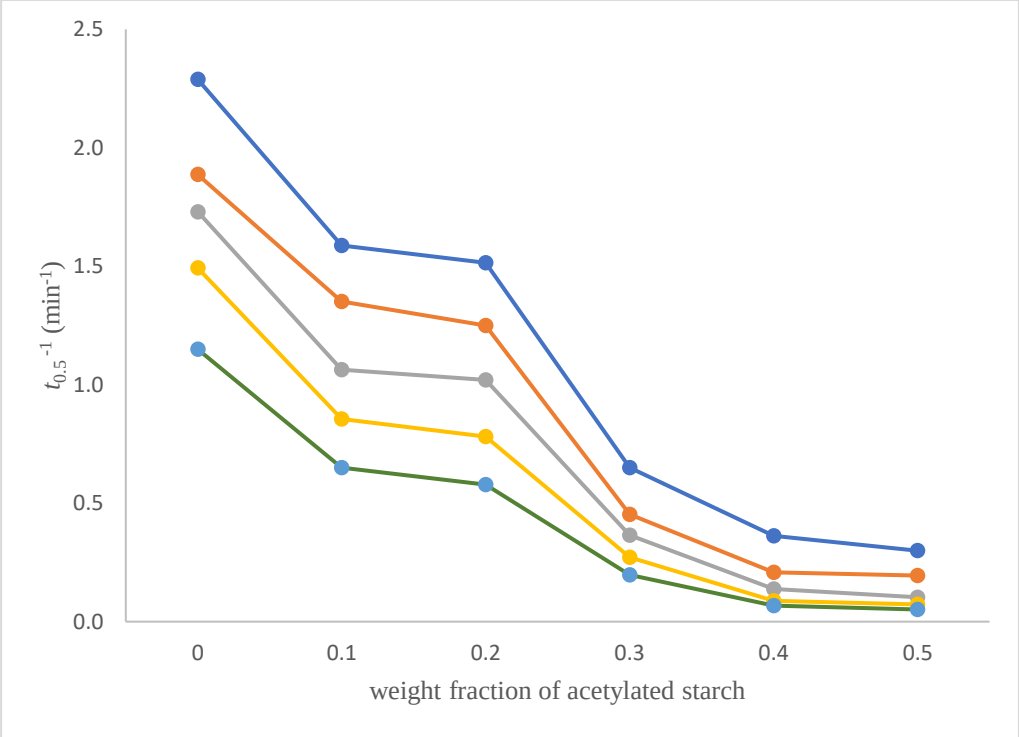

Figure 4.15: Reciprocal of half-time of crystallization, $t_{0.5}^{-1}$ versus weight fraction of acetylated starch for different ratios of PEO/acetylated rice starch blends at T_cs: (●) 40.0 °C, (●) 41.0 °C, (●) 42.0 °C, (●) 43.0 °C, (●) 44.0 °C.

4.3.3 Estimation of equilibrium melting temperatures, T_m° of pure PEO and PEO in the blends

The equilibrium melting temperature, T_m° is the melting point of crystals that have an extended chain structure and are in their most perfect state (Chung, Yeh, and Hong, 2002). Understanding T_m° is particularly crucial for comprehending the crystallization mechanism. This is because, according to

Okeda, Ogawa, and Matsumoto (2006), the rate of undercooling, $\Delta T = T_m^\circ - T_c$, determines crystallization phenomena like lateral growth rate and nucleation rate, for which data on both T_m° and T_c are needed.

One of the methods most frequently used to determine T_m° is the Hoffman-Weeks method. The Hoffman-Weeks method is regarded as an easy process with broad applicability because it only requires the experimental melting temperature, T_m, of the crystallites formed at a specific T_c (Soccio et al., 2011). The samples were initially crystallized isothermally for five half-times of crystallization, $t_{0.5}$, at different crystallization temperatures, T_c. Using the first derivative of the melting peak, the observed melting temperatures of pure PEO and PEO in the blends at various crystallization temperatures can then be determined. The T_m° of pure PEO and PEO in the blends were then estimated using the Hoffman-Weeks equation, as shown by Equation 4.8 (Hoffman and Miller, 1997).

$$T_m = \left(\frac{1}{\gamma}\right)T_c + \left(1 - \frac{1}{\gamma}\right)T_m^\circ \qquad \text{(Equation 4.8)}$$

where the stability parameter, which is affected by the lamellar thickness, is denoted by $1/\gamma$. $1/\gamma$ has a value that ranges from 0 to 1. When $1/\gamma$ approaches 0, the polymer crystals are deemed stable, and when $1/\gamma$ approaches 1, they are deemed unstable.

The graph of T_m versus T_c for various blends are shown in Figure 4.16. The slope of the plot is used to estimate $1/\gamma$ while an estimate of the T_m° of a sample can be obtained from the intersection point by extrapolating the curve of T_m versus T_c to the line $T_m = T_c$. The T_m° for pure PEO was estimated to be 65.4°C.

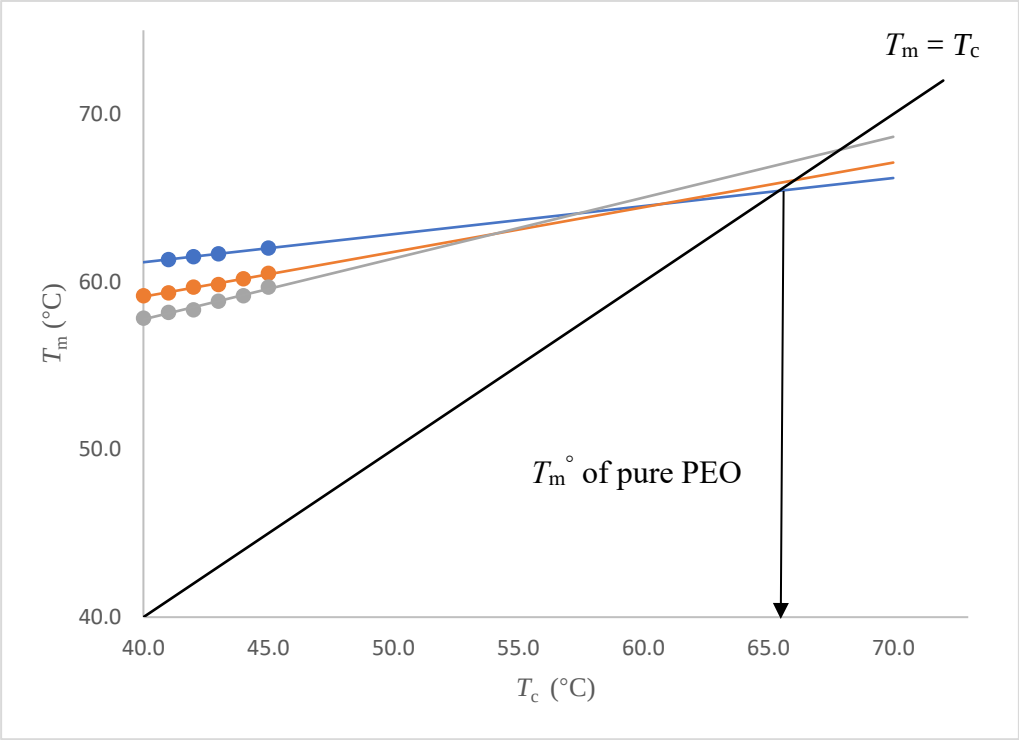

Figure 4.16: Hoffman-Weeks plots for (●) pure PEO, (●) 80/20 and (●) 60/40 PEO/acetylated rice starch blends.

It should be noted that there is a linear relationship between the T_m and T_c; that is, as T_c increased, T_m also increased. Re-crystallization processes or secondary crystallization mechanisms may be involved at elevated T_c (within a certain range), producing more perfect crystals that require more energy to melt and, consequently, a higher T_m was obtained (Antonio G.B. Pereira et al., 2009).

Table 4.2 lists the equilibrium melting temperatures (T_m°s) and stability parameters (1/γ) obtained for various PEO/acetylated starch blend compositions. The Hoffman Weeks plots' slopes for the PEO/acetylated starch blends yielded stability parameters that ranged from 0.10 to 0.31. Since the values were closer to zero, it can be concluded that the crystals formed during crystallization were stable. The T_m° for PEO/acetylated rice starch blend was higher than pure PEO except for 50/50 polymer blend. According to Wiley (2015), when bulky groups were present in the polymer chains, the chain flexibility will be restricted, thus increased the melting temperature.

In addition, a strong hydrogen bond formed between polymer chains and starch particles, further limited the chain mobility and delayed chain melting (Hossein Baniasadi et al., 2023). However, for 50/50 PEO/acetylated starch blend, a depression in T_m° was observed. This was because the reduction in melting point was closely linked to a significant drop in crystallinity content (St-Onge et al., 2021). Thus, for 50/50 PEO/acetylated starch blend, the crystalline region in PEO was much more diluted by the high concentration of the acetylated rice starch.

Table 4.2: Equilibrium melting temperatures, T_m°s, and stability parameters, 1/γ for various compositions of PEO/acetylated rice starch blends.

PEO/acetylated rice starch blend	Equilibrium melting temperature, T_m° (°C)	Stability parameter, 1/γ
100/0	65.4	0.167
90/10	69.3	0.089
80/20	66.1	0.267
70/30	65.9	0.309
60/40	67.9	0.363
50/50	63.1	0.215

4.3.4 Determination of nucleation parameter, K_g for pure PEO and PEO/acetylated rice starch blend

The energy required to form a secondary nucleus of a critical size is known as the nucleation parameter, K_g (Nikola Kocic et al., 2014). K_g is often determined in the study of the relationship between the morphology of polymers and the crystallization process. The relationship between K_g and the reciprocal of the half-time of crystallization, $t_{0.5}^{-1}$, can be characterized as Arrhenius-like in accordance with the Hoffman theory (Hoffman et al., 1975).

$$t_{0.5}^{-1} = \exp\left(-K_g \frac{T_m^\circ}{T_c \Delta T}\right) \qquad \text{(Equation 4.9)}$$

T_m° is the equilibrium melting temperature of pure PEO, which is 65.4 °C; K_g represents the nucleation parameter; and ΔT denotes undercooling, which is calculated by subtracting T_c from T_m°. By taking the natural logarithm on both sides of the Equation 4.9, the equation will be rearranged to produce Equation 4.10.

$$\ln\ t_{0.5}^{-1} = \left(-K_g \frac{T_m^\circ}{T_c \Delta T}\right) \qquad \text{(Equation 4.10)}$$

Graph of $ln\ t_{0.5}^{-1}$ plotted against $\left(\frac{T_m^\circ}{T_c \Delta T}\right)$ for pure PEO with a negative slope is depicted in Figure 4.17. The nucleation parameter, K_g, can be determined from the slope of the plot.

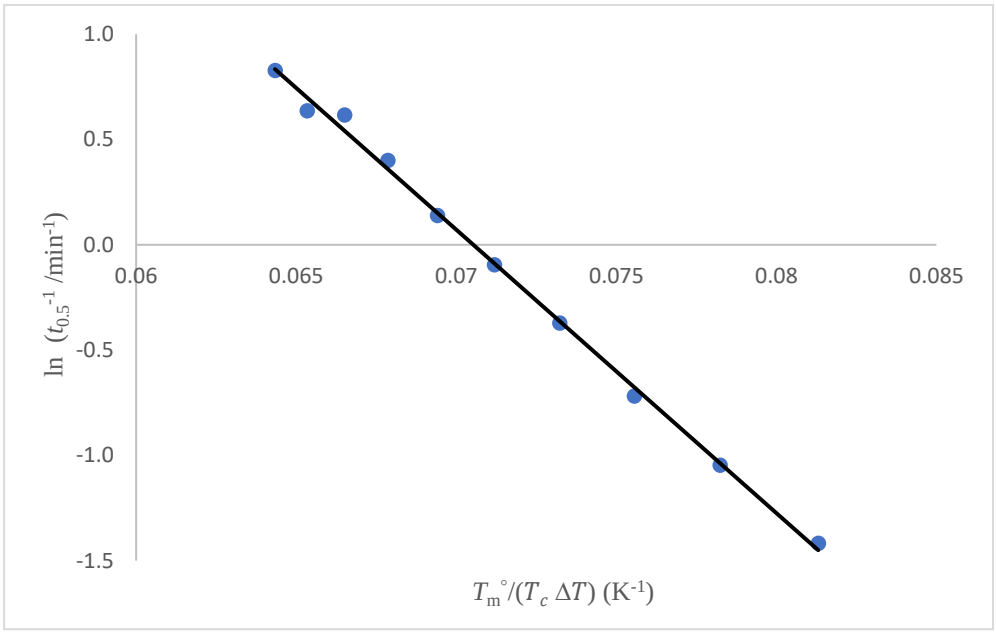

Figure 4.17: Graph of ln $t_{0.5}^{-1}$ versus $T_m^\circ/T_c\ \Delta T$ for pure PEO.

The nucleation parameter, K_g of pure PEO was determined to be 134.6 K. Table 4.3 summarizes the K_g of different PEO/acetylated rice starch blends' compositions. The value of K_g was found to increase with increasing the amount of acetylated rice starch which showed that adding acetylated starch increased the amount of energy needed to form the secondary nucleus because PEO's chain mobility was restricted.

Table 4.3: Nucleation parameters, K_g for pure PEO and different PEO/acetylated rice starch blends' compositions.

PEO/acetylated rice starch blend	Nucleation parameters, K_g (K)
100/0	134.6
80/20	186.0
70/30	196.7
60/40	360.9

4.3.5 Determination of the polymer-polymer interaction parameter, χ_{12} of PEO/acetylated starch blend

Gaining an understanding of the melting and crystallization behavior of a crystalline or amorphous polymer blend can offer valuable insights into the miscibility and interactions of the blend's components. It is important to recognize that the crystallization of the blend does not necessarily indicate phase separation in the polymer melt. The Nishi-Wang equation, as presented in

Equation 4.11, is used to estimate the interaction parameter, χ_{12}, for the components in a binary polymer blend, which reflects the miscibility of the polymers in the blend (Nishi and Wang, 1975).

$$\left(\frac{1}{T_m^o(PEO)} - \frac{1}{T_m^o(blend)}\right) = \frac{Rv_1}{\Delta H^o v_2}\left[\frac{ln\phi_1}{m_1} + \left(\frac{1}{m_1} + \frac{1}{m_2}\right) + \chi_{12}\phi_2^2\right] \quad \text{(Equation 4.11)}$$

T_m° (blend) and T_m° (PEO) represent the equilibrium melting temperatures of PEO in the PEO/acetylated starch blends and pure PEO, respectively. R is the universal gas constant, with a value of 8.314 J mol^{-1} K^{-1}; v_1 and v_2 are the molar volumes of PEO and acetylated rice starch, respectively; ΔH° is the heat of fusion per mole of repeating unit for the perfectly crystallizable polymer, with a value of 7600 J mol^{-1} K^{-1} (Pereira et al., 2010); ϕ_1 and ϕ_2 denote the volume fractions of PEO and acetylated rice starch, respectively; m_1 and m_2 indicate the degrees of polymerization for PEO and acetylated rice starch, respectively; and χ_{12} is the polymer-polymer interaction parameter. Since m_1 and m_2 are large for high molecular weight polymers, they can be disregarded. Equation 4.12 can be obtained by simplifying the Nishi-Wang equation.

$$\left(\frac{1}{T_m^o(PEO)} - \frac{1}{T_m^o(blend)}\right) = \frac{Rv_1}{\Delta H^o v_2}\chi_{12}\phi_2^2 \quad \text{(Equation 4.12)}$$

Figure 4.18 illustrates the Nishi Wang plot of $\left(\frac{1}{T_m^o(PEO)} - \frac{1}{T_m^o(blend)}\right)$ against ϕ_2^2, the slope of the curve can be used to determine the polymer-polymer interaction parameter, χ_{12} (Kim et al., 2021). Phase separation in the polymer

blend system occurs if χ_{12} is positive, ($\chi_{12} > 0$), indicating that the polymer blend is immiscible. If χ_{12} is negative, ($\chi_{12} < 0$), the polymer blend is miscible (Pereira et al., 2010). It was estimated that χ_{12} had a value of 0.489. PEO and acetylated rice starch blends exhibited immiscibility as a result of the positive value of of χ_{12}. The correlation coefficient, r^2, was low. This could have been due to experimental error, as the sample was kept for an extended period before conducting the miscibility study. The samples may have absorbed water, which likely introduced errors into the results.

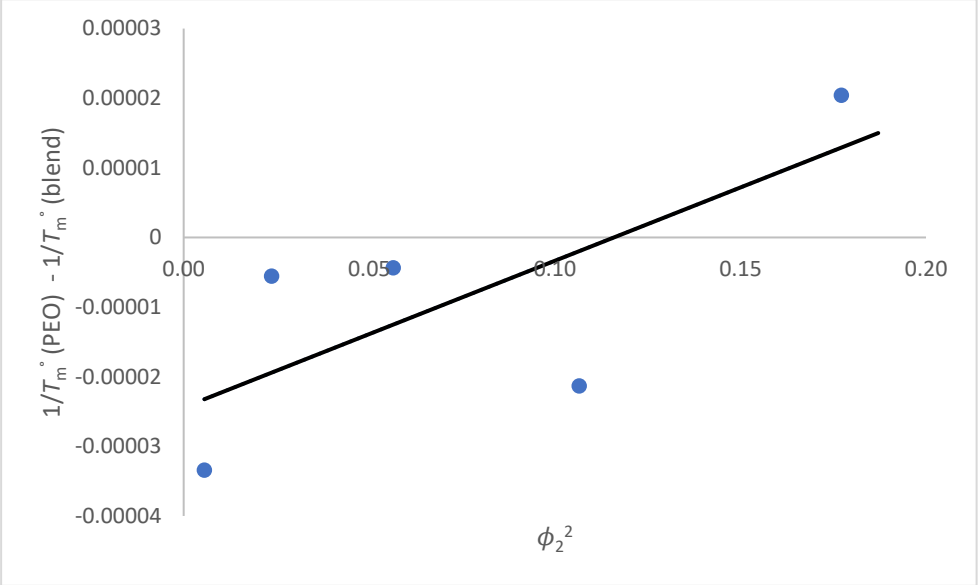

Figure 4.18: Plot of $\left(\frac{1}{T_m^o(PEO)} - \frac{1}{T_m^o(blend)}\right)$ against ϕ_2^2 for PEO/acetylated rice starch blends.

CHAPTER 5

CONCLUSION

With the aid of iodine as a catalyst and acetic anhydride as the esterifying agent, rice starch was successfully acetylated. The rice starch's successful acetylation was confirmed using Attenuated Total Reflectance-Fourier Transform Infrared (ATR-FTIR) spectroscopy. Successful acetylation of rice starch was verified by the appearance of some new peaks at 1732 cm^{-1}, 1369 cm^{-1}, and 1226 cm^{-1} representing the stretching vibration of ester carbonyl group (C=O), CH_3, and C-O in the acetyl group respectively.

Using the back-titration method, the degree of substitution (DS) of rice starch was ascertained, and several parameters influenced the DS of rice starch were investigated. The highest DS was observed in the acetylated rice starches produced with a 1:4 molar ratio of starch to acetic anhydride, a 0.25 mmol iodine concentration, and a reaction time of two minutes.

The solution casting method was used to prepare various compositions of PEO/acetylated rice starch blends using the highest DS acetylated rice starch. Differential scanning calorimetry (DSC) was used to examine the isothermal crystallization and melting behavior of the PEO/acetylated rice starch blends.

The overall crystallinity, X_c of PEO decreased as acetylated rice starch contents increased, suggesting that higher acetylated rice starch contents in the blends reduced PEO nucleation and crystal growth. The Avrami equation was utilized to investigate the isothermal crystallization kinetics. The crystallization rate was found to decrease with increasing crystallization temperature. The blends of PEO and acetylated rice starch showed two-dimensional crystal growth geometry, as indicated by the Avrami exponent, n_A values, which varied from 1.50 to 1.82. Furthermore, due to the addition of acetylated rice starch reduced chain flexibility, it was observed that the rate of crystallization decreased as the weight fraction of acetylated rice starch increased.

Hoffman-Weeks method was used to estimate the equilibrium melting temperatures, T_m°, of pure PEO and PEO in the blends. The T_m° of pure PEO was estimated to be 65.4 °C. For all PEO/acetylated rice starch blends except the 50/50 blend composition, there was an increase in the equilibrium melting temperature of PEO in the blends. Besides that, the nucleation parameters, K_g increased when acetylated rice starch content increased.

Based on the polymer-polymer interaction parameter, χ_{12}, the miscibility of the PEO/acetylated rice starch blends was estimated using the Nishi-Wang equation. The χ_{12} was found to be 0.489. This positive value indicated that the PEO and acetylated rice starch were immiscible in the blend compositions under investigation.

Further studies on PEO/acetylated rice starch blends are needed to better understand the non-isothermal crystallization and mechanical properties of the blends. Further study could investigate the miscibility through glass transition temperature, T_g, measurements of the blends. Another potential area of investigation is determining the interaction between PEO and acetylated rice starch based on crystal size change approach using X-ray diffraction (XRD).

REFERENCES

Abe, M.M., Martins, J.R., Sanvezzo, P.B., Macedo, J.V., Branciforti, M.C., Halley, P., Botaro, V.R. and Brienzo, M., 2021. Advantages and disadvantages of bioplastics production from starch and lignocellulosic components. *Polymers*, [e-journal] 13(15), pp.2484. https://doi.org/10.3390/polym13152484.

Abioye, A.A. and Obuekwe, C.C., 2020. Investigation of the biodegradation of low-density polyethylene-starch bi-polymer blends. *Results in Engineering*, [e-jorunal] 5, pp.100090. https://doi.org/10.1016/j.rineng.2019.100090.

Amer Ali Mahdi et al., 2023. Replacement of polyethylene oxide by peach gum to produce an active film using Litsea cubeba essential oil and its application in beef. *International journal of biological macromolecules*, [e-journal] 241, pp.124592–124592. https://doi.org/10.1016/j.ijbiomac.2023.124592.

Amigo, N. et al., 2019. Effect of starch nanoparticles on the crystallization kinetics and photodegradation of high density polyethylene. *Composites Part B Engineering*, [e-journal] 174, pp.106979–106979. https://doi.org/10.1016/j.compositesb.2019.106979.

Antonio G.B. et al., 2009. Polymer blends based on PEO and starch: Miscibility and spherulite growth rate evaluated through DSC and optical microscopy. *Materials science & engineering. C, Biomimetic materials, sensors and systems (Print)*, [e-journal] 29(2), pp.499–504. https://doi.org/10.1016/j.msec.2008.09.009.

Araneda, E. et al., 2011. Crystallization behavior of PEO in blends of poly(ethylene oxide)/poly(2-vinyl pyridine)-*b*-(ethylene oxide) block copolymer. *SPE transactions/Polymer engineering and science*, [e-journal] 52(5), pp.1128–1136. https://doi.org/10.1002/pen.22183.

Ariyantoro, A., Katsuno, N. and Nishizu, T., 2018. Effects of dual modification with succinylation and annealing on physicochemical, thermal and morphological properties of corn starch. *Foods*, [e-journal] 7(9), pp.133. https://doi.org/10.3390/foods7090133.

Atiwesh, G., Mikhael, A., Parrish, C.C., Banoub, J. and Le, T.-A.T., 2021. Environmental impact of bioplastic use: A review. *Heliyon*, [e-journal] 7(9). https://doi.org/10.1016/j.heliyon.2021.e07918.

Avrami, M., 1939. Kinetics of phase change. I general theory. *The Journal of Chemical Physics*, [e-journal] 7(12), pp.1103–1112. https://doi.org/10.1063/1.1750380.

Behera, K., Chang, Y.H., Yadav, M. and Chiu, F.C., 2020. Enhanced thermal stability, toughness, and electrical conductivity of carbon nanotube-reinforced biodegradable poly(lactic acid)/poly(ethylene oxide) blend-based nanocomposites. *Polymer*, [e-journal] 186, pp.122002. https://doi.org/10.1016/j.polymer.2019.122002.

Bhatt, P. et al., 2022. Structural modifications and strategies for native starch for applications in advanced drug delivery. *BioMed Research International*, [e-journal] 2022, pp.e2188940. https://doi.org/10.1155/2022/2188940.

Biswas, A. et al., 2007. Iodine catalyzed esterification of cellulose using reduced levels of solvent. *Carbohydrate Polymers*, [e-journal] 68(3), pp.555–560. https://doi.org/10.1016/j.carbpol.2006.10.018.

Biswas, A. et al., 2009. Iodine-catalyzed esterification of polysaccharides. *Chemistry Today*, [e-journal] 27(4), pp.33–35.

Chandran, C. S., Shanks, R. and Thomas, S., 2014. Polymer Blends. In: Chandran, C. S., Shanks, R. and Thomas, S., eds. *Nanostructured Polymer Blends*. Amsterdam: Elsevier. pp. 1-14.

Chi, H. et al., 2008. Effect of acetylation on the properties of corn starch. *Food Chemistry*, [e-journal] 106(3), pp.923–928. https://doi.org/10.1016/j.foodchem.2007.07.002.

Chuah, K.P., Gan, S.N. and Chee, K.K., 1999. Determination of avrami exponent by differential scanning calorimetry for non-isothermal crystallization of polymers. *Polymer*, [e-jounal] 40(1), pp.253–259. https://doi.org/10.1016/s0032-3861(98)00188-8.

Chung, W.T., Yeh, W.J. and Hong, P.D., 2002. Melting behavior of poly(trimethylene terephthalate). *Journal of Applied Polymer Science*, [e-jounal] 83(11), pp.2426–2433. https://doi.org/10.1002/app.10206.

Compart, J., Singh, A., Joerg, F., and Ardha. A., 2023. Customizing starch properties: A review of starch modifications and their applications. *Polymers*, [e-journal]15(16), pp.3491–3491. https://doi.org/10.3390/polym15163491.

Crompton, T. R., 2006. Polymer Reference Book. [e-book] United Kingdom: Rapra Technology Limited. Available at: Google Books [Accessed 16 August 2024]

Dimitrov, I. and Tsvetanov, C.B., 2012. High-Molecular-Weight Poly(ethylene oxide). *Polymer Science: A Comprehensive Reference*, [e-journal] pp.551–569. https://doi.org/10.1016/b978-0-444-53349-4.00100-x.

Ding, Y. et al., 2020. Study on compatible characteristics of wheat and purple sweet potato starches. *Food Hydrocolloids*, [e-journal] 107, pp.105961–105961. https://doi.org/10.1016/j.foodhyd.2020.105961.

Diop, C.I.K., Li, H.L., Xie, B.J. and Shi, J., 2011. Impact of the catalytic activity of iodine on the granule morphology, crystalline structure, thermal properties and water solubility of acetylated corn (Zea mays) starch synthesized under microwave assistance. *Industrial Crops and Products*, [e-journal] 33(2), pp.302–309. https://doi.org/10.1016/j.indcrop.2010.11.018.

Foreman, J. and Blaine, R.L., 1995. Isothermal crystallization made easy: A simple model and modest cooling rates. *ANTEC'95*., 2, pp.2409-2412.

Hoffman, J.D., Frolen, L.J., Ross, G.S. and Lauritzen, J.I., 1975. On the growth rate of spherulites and axialites from the melt in polyethylene fractions: Regime I and regime II crystallization. *Journal of Research of the National Bureau of Standards Section A Physics and Chemistry*, [e-journal] 79(6), pp.671–671. https://doi.org/10.6028/jres.079a.026.

Hoffman, J.D. and Miller, R.L., 1997. Kinetic of crystallization from the melt and chain folding in polyethylene fractions revisited: theory and experiment. *Polymer*, [e-journal] 38(13), pp.3151–3212. https://doi.org/10.1016/s0032-3861(97)00071-2.

Höhne, G., Hemminger, W. F. and Flammersheim, H. J., 2013. Differential scanning calorimetry. [e-book] New York: Springer Science & Business Media. Available at: Google Books [Accessed 28 July 2024].

Hossein Baniasadi et al., 2023. Heat-induced actuator fibers: Starch-containing biopolyamide composites for functional textiles. *ACS Applied Materials & Interfaces*, [e-journal] 15(41), pp.48584–48600. https://doi.org/10.1021/acsami.3c08774.

Hussein, A., 2022. *Essentials of flow assurance solids in oil and gas operations: Understanding Fundamentals, characterization, prediction, environmental safety, and Management*. Amsterdam: Gulf Professional Publishing.

Imre, B. and Vilaplana, F., 2020. Organocatalytic esterification of corn starches towards enhanced thermal stability and moisture resistance. *Green Chemistry*, [e-journal] 22(15), pp.5017–5031.https://doi.org/10.1039/d0gc00681e.

Jayarathna, S., Andersson, M. and Andersson, R., 2022. Recent advances in starch-based blends and composites for bioplastics applications. *Polymers*, [e-journal] 14(21), pp.4557. https://doi.org/10.3390/polym14214557.

Kai, D., Liow, S.S. and Loh, X.J., 2014. Biodegradable polymers for electrospinning: Towards biomedical applications. *Materials Science and Engineering: C*, [e-journal] 45, pp.659–670. https://doi.org/10.1016/j.msec.2014.04.051.

Kalia, S. and Avérous, L., 2012. *Biopolymers: Biomedical and environmental applications*. Hoboken, N.J: Wiley.

Kalkar, A.K. and Deshpande, A.A., 2001. Kinetics of isothermal and non-isothermal crystallization of poly(butylene terephthalate)/ liquid crystalline polymer blends. *Polymer Engineering & Science*, [e-journal] 41(9), pp.1597–1615. https://doi.org/10.1002/pen.10858.

Kalkar, A.K., Deshpande, V.D. and Kulkarni, M.J., 2008. Isothermal crystallization kinetics of poly(phenylene sulfide)/TLCP composites. *Polymer Engineering and Science*, [e-journal] 49(2), pp.397–417. https://doi.org/10.1002/pen.21263.

Kim, H.J., Peng, X., Shin, Y., Hillmyer, M.A. and Ellison, C.J., 2021. Blend miscibility of poly(ethylene terephthalate) and aromatic polyesters from salicylic acid. *The journal of physical chemistry B*, [e-jounal] 125(1), pp.450–460. https://doi.org/10.1021/acs.jpcb.0c09322.

Kong, Y. and Hay, J.N., 2002. The measurement of the crystallinity of polymers by DSC. *Polymer*, [e-journal] 43(14), pp.3873–3878. https://doi.org/10.1016/s0032-3861(02)00235-5.

Kwon, S., Kim, Y., Jang, H., Sun Jong Kim and Park, S., 2022. Poly (ethylene oxide) (PEO) influence on mechanical, thermal, and degradation properties of PLA/PBSeT blends. *Journal of applied polymer science*, [e-journal] 140(2). https://doi.org/10.1002/app.53299.

Lewicka, K., Siemion, P. and Kurcok, P., 2015. Chemical modifications of starch: Microwave effect. *International Journal of Polymer Science*, 2015, pp.1–10. https://doi.org/10.1155/2015/867697.

Li, B., Liu, J., Yu, B. and Zheng, X., 2022. The environmental impact of plastic grocery bags and their alternatives. *IOP Conference Series: Earth and Environmental Science*, [e-journal] 1011(1), pp.012050. https://doi.org/10.1088/1755-1315/1011/1/012050.

Li, D. et al., 2023. The role of the interface of PLA with thermoplastic starch in the nonisothermal crystallization behavior of PLA in PLA/Thermoplastic Starch/SiO_2 Composites. *Polymers*, [e-journal] 15(6), pp.1579–1579. https://doi.org/10.3390/polym15061579.

Li, J. et al., 2009. Microwave-assisted solvent-free acetylation of cellulose with acetic anhydride in the presence of iodine as a catalyst. *Molecules*, [e-journal] 14(9), pp.3551–3566. https://doi.org/10.3390/molecules14093551.

Lin, D. et al., 2019. Study on preparation and physicochemical properties of hydroxypropylated starch with different degree of substitution under microwave assistance. *International journal of biological macromolecules*, [e-journal] 125, pp.290–299. https://doi.org/10.1016/j.ijbiomac.2018.12.031.

Liu, W., Wang, Y.-J. and Sun, Z., 2004. Crystallization behavior of starch-filled polypropylene. *Journal of Applied Polymer Science*, [e-journal] 92(1), pp.484–492. https://doi.org/10.1002/app.20019.

Liu, X.L., Zhu, C.F., Liu, H.C. and Zhu, J.M., 2022. Quantitative analysis of degree of substitution/molar substitution of etherified polysaccharide derivatives. *Designed Monomers and Polymers*, [e-journal] 25(1), pp.75–88. https://doi.org/10.1080/15685551.2022.2054118.

Li, X., 1985. Studies of the crystallization behavior in the crystalline/amorphous polymer blends: poly(ethylene oxide)/poly(methyl methacrylate) and poly(ethylene oxide)/poly(vinyl acetate). *Polymer Communications*, 3, pp. 280-288.

Li, Y., et al., 2020. A composite solid polymer electrolyte incorporating MnO_2 nanosheets with reinforced mechanical properties and electrochemical stability for lithium metal batteries. *Journal of Materials Chemistry A*, [e-journal] 8(4), pp.2021–2032. https://doi.org/10.1039/c9ta11542k.

Lorenzo and Silvestre, C., 1999. Non-isothermal crystallization of polymers. *Progress in Polymer Science,* [e-journal] 24(6), pp.917–950. https://doi.org/10.1016/s0079-6700(99)00019-2.

Lu, Y., Tang, Y. and Xia, X., 2018. Non-isothermal crystallization of copper-containing composite based on polymer alloy of poly(ethylene oxide) and polyethylene. *Thermochimica acta*, [e-journal] 670, pp.61–70. https://doi.org/10.1016/j.tca.2018.10.007.

Maha, N. and Muhammed, S., 2023. Synthesis, characterization and antimicrobial study of polyacetal-co complex/nano chitosan polymer blend. *Journal of Wasit for Science and Medicine* [e-journal] 16(3), pp.44–51. https://doi.org/10.31185/jwsm.476.

Marichelvam, M.K., Jawaid, M. and Asim, M., 2019. Corn and rice starch-based bio-plastics as alternative packaging materials. *Fibers*, [e-journal] 7(4), pp.32. https://doi.org/10.3390/fib7040032.

Masina, N. et al., 2017. A review of the chemical modification techniques of starch. *Carbohydrate Polymers*, [e-journal] 157, pp.1226–1236. https://doi.org/10.1016/j.carbpol.2016.09.094.

Namazi, H., 2017. Polymers in our daily life. *BioImpacts*, [e-journal] 7(2), pp.73–74. https://doi.org/10.15171/bi.2017.09.

Nešić, A., Cabrera-Barjas, G., Dimitrijević-Branković, S., Davidović, S., Radovanović, N. and Delattre, C., 2019. Prospect of polysaccharide-based materials as advanced food packaging. *Molecules*, [e-journal] 25(1), pp.135. https://doi.org/10.3390/molecules25010135.

Nikola Kocic, Lederhofer, S., Kretschmer, K., Bastian, M. and Heidemeyer, P., 2014. Nucleation parameter and size distribution of critical nuclei for nonisothermal polymer crystallization: The influence of the cooling rate and filler. *Journal of Applied Polymer Science*, [e-journal] 132(6), pp. 1-15. https://doi.org/10.1002/app.41433.

Nishi, T. and Wang, T.T., 1975. Melting point depression and kinetic effects of cooling on crystallization in poly(vinylidene fluoride)-poly(methyl methacrylate) mixtures. *Macromolecules*, [e-journal] 8(6), pp.909–915. https://doi.org/10.1021/ma60048a040.

Ogunsona, E., Ojogbo, E. and Mekonnen, T., 2018. Advanced material applications of starch and its derivatives. *European Polymer Journal*, [e-journal] 108, pp.570–581. https://doi.org/10.1016/j.eurpolymj.2018.09.039.

Okeda, M., Ogawa, Y. and Matsumoto, N., 2006. Equilibrium melting temperature of aliphatic polyesters using model compounds. *Polymer Journal*, [e-jounal] 38(10), pp.1089–1092. https://doi.org/10.1295/polymj.pj2006064.

Olabis, O., 2012. *Polymer-polymer miscibility*. Burlington: Elsevier Science.

Panapitiya, N. et al., 2016. Compatibilized immiscible polymer blends for gas separations. *Materials*, [e-journal] 9(8), pp.643. https://doi.org/10.3390/ma9080643.

Parameswaranpillai, J., Thomas, S. and Grohens, Y., 2014. Polymer blends: State of the art, new challenges, and opportunities. *Characterization of Polymer Blends*, [e-journal] pp.1–6. https://doi.org/10.1002/9783527645602.ch01.

Pereira, B., Paulino, A.T., Rubira, A.F. and Muniz, E.C., 2010. Polymer-polymer miscibility in PEO/cationic starch and PEO/hydrophobic starch blends. *Express polymer letters*, [e-journal] 4(8), pp.488–499. https://doi.org/10.3144/expresspolymlett.2010.62.

Qiu, Z., Yang, W., Ikehara, T. and Nishi, T., 2005. Miscibility and crystallization behavior of biodegradable blends of two aliphatic polyesters. Poly(3-hydroxybutyrate-co-hydroxyvalerate) and poly(ε-caprolactone). *Polymer*, [e-journal] 46(25), pp.11814–11819. https://doi.org/10.1016/j.polymer.2005.10.058.

Ramírez-Arreola, D.E. et al., 2009. Rapid starch acetylation at low temperature using iodine as catalyst. *Macromolecular symposia*, [e-journal] 283–284(1), pp.174–180. https://doi.org/10.1002/masy.200950923.

Rohindra, D.R. and Khurma, J.R., 2007. Miscibility, melting and crystallization of poly(ε-caprolactone) and poly (vinyl formal) blend. *South Pacific journal of natural and applied sciences*, 25(1), pp.53–53. https://doi.org/10.1071/sp07009.

Samir, A., Ashour, F.H., Hakim, A.A.A. and Bassyouni, M., 2022. Recent advances in biodegradable polymers for sustainable applications. *npj Materials Degradation*, [e-journal] 6(1). https://doi.org/10.1038/s41529-022-00277-7.

Singh, J., Kaur, L. and McCarthy, O.J., 2007. Factors influencing the physico-chemical, morphological, thermal and rheological properties of some chemically modified starches for food applications—A review. *Food Hydrocolloids*, [e-journal] 21(1), pp.1–22. https://doi.org/10.1016/j.foodhyd.2006.02.006.

Singh, V., Ali, S.Z., Somashekar, R. and Mukherjee, P.S., 2006. Nature of crystallinity in native and acid modified starches. *International Journal of Food Properties*, [e-journal] 9(4), pp.845–854. https://doi.org/10.1080/10942910600698922.

Soccio, M., Lotti, N., Finelli, L. and Munari, A., 2011. Equilibrium melting temperature and crystallization kinetics of α- and β′-PBN crystal forms. *Polymer Journal*, [e-journal] 44(2), pp.174–180. https://doi.org/10.1038/pj.2011.112.

Somsunan, R. and Mainoiy, N., 2019. Isothermal and non-isothermal crystallization kinetics of PLA/PBS blends with talc as nucleating agent. *Journal of Thermal Analysis and Calorimetry*. [e-journal] 139(1), pp. 1941-1948. https://doi.org/10.1007/s10973-019-08631-9.

St-Onge, V., Cui, M., Rochon, S., Daigle, J.-C. and Claverie, J.P., 2021. Reducing crystallinity in solid polymer electrolytes for lithium-metal batteries via statistical copolymerization. *Communications Materials*, [e-journal] 2(1), pp.1–11. https://doi.org/10.1038/s43246-021-00187-2.

Surendren, A., Mohanty, A.K., Liu, Q. and Misra, M., 2022. A review of biodegradable thermoplastic starches, their blends and composites: recent developments and opportunities for single-use plastic packaging alternatives. *Green Chemistry*, [e-journal] 24(22), pp.8606–8636. https://doi.org/10.1039/d2gc02169b.

Tamaño-Machiavello, M.N. et al., 2017. Crystallization kinetics of poly(ethylene oxide) confined in semicrystalline poly(vinylidene) fluoride. *Journal of Polymer Science Part B Polymer Physics*, [e-journal] 56(7), pp. 588–597. https://doi.org/10.1002/polb.24564.

Thakur, V. K. and Kessler, M. R. eds., 2015. *Liquid crystalline polymers: Volume 1 – structure and chemistry.* [e-book] Switzerland: Springer. Available at: Google Books < https://books.google.com/> [Accessed 11 August 2024].

Tippabattini Jayaramudu, Ko, H.-U., Hyun Chan Kim, Kim, J., Eun Sik Choi and Kim, J., 2019. Adhesion properties of poly(ethylene oxide)-lignin blend for nanocellulose composites. *Composites Part B*, [e-journal] 156, pp.43–50. https://doi.org/10.1016/j.compositesb.2018.08.063.

Wiley, J., 2015. Physical, thermal, and mechanical properties of polymers. *Biosurfaces*, [e-journal] pp.329–344. https://doi.org/10.1002/9781118950623.app1.

Xue, Z., He, D. and Xie, X., 2015. Poly(ethylene oxide)-based electrolytes for lithium-ion batteries. *Journal of Materials Chemistry A*, [e-journal] 3(38), pp.19218–19253. https://doi.org/10.1039/C5TA03471J.

Xu, J., Reiter, G. and Alamo, R.G., 2021. Concepts of nucleation in polymer crystallization. *Crystals*, [e-journal] 11(3), pp.304. https://doi.org/10.3390/cryst11030304.

Xu, Y., Vesselin Miladinov and Hanna, M.A., 2004. Synthesis and characterization of starch acetates with high substitution. *Cereal Chemistry*, 81(6), pp.735–740. https://doi.org/10.1094/cchem.2004.81.6.735.

Yang, Q. et al., 2017. Effect of microwave irradiation on internal molecular structure and physical properties of waxy maize starch. *Food Hydrocolloids*, [e-journal] 69, pp.473–482. https://doi.org/10.1016/j.foodhyd.2017.03.011.

Zhang, H., Wang, R., Wang, J. and Dong, Y., 2013. Microwave-assisted synthesis and characterization of acetylated corn starch. *Starch - Stärke*, [e-journal] 66(5-6), pp.515–523. https://doi.org/10.1002/star.201300165.

Zhao, K. et al., 2018. Microwave pretreated esterification improved the substitution degree, structural and physicochemical properties of potato starch esters. *LWT-Food Sci. Technol,* [e-journal] 90, pp.116–123. https://doi.org/10.1016/j.lwt.2017.12.021.

APPENDIX A

A.1 Data for degree of substitution of acetylated rice starch

A.1.1 Data for Figure 4.6

Starch to acetic anhydride ratio	Degree of substitution of starch
1:2	1.144
1:3	1.886
1:4	2.377
1:5	1.773

A.1.2 Data for Figure 4.7

Amount of iodine (mmol)	Degree of substitution of starch
0.05	0.508
0.10	1.030
0.25	1.886
0.50	1.805
0.75	1.777

A.1.3 Data for Figure 4.8

Reaction time (mins)	Degree of substitution of starch
1	0.658
2	1.886
3	1.330
4	0.956
5	0.772

APPENDIX B

B.1 Degree of crystallinity, X_c for PEO/acetylated rice starch blends

The degrees of crystallinity, X_c of PEO and PEO in the blends are calculated using the following equation:

$$X_c = \frac{\Delta H_m}{\Delta H_m^0 \times w_{PEO}} \times 100\ \%$$

where ΔH_m and ΔH°_m are the melting enthalpies of the PEO in the blends and 100 % crystalline of PEO, and w_{PEO} is the weight fraction of PEO in the PEO/acetylated rice starch blends. ΔH°_m was found in the literature to be 196.6 J/g.

B.1.1 Example of calculation of degree of crystallinity, X_c for pure PEO at crystallization temperature, T_c = 40.0 °C

For pure PEO,

ΔH°_m = 196.6 J/g

ΔH_m = 124.2 J/g

w_{PEO} = 1.0

$X_c = \frac{\Delta H_m}{\Delta H_m^0 \text{ x } w_{PEO}}$ x 100 %

$= \frac{124.2\ J/g}{196.6\ J/g \text{ x } 1.0}$ x 100 %

= 63.2 %

B.1.2 Data for Figure 4.9

Weight fraction of acetylated rice starch	Degree of crystallinity, X_c (%)
0.0	63.2
0.1	64.2
0.2	66.3
0.3	59.2
0.4	52.7
0.5	50.1

APPENDIX C

C.1 Data for isothermal crystallisation of pure PEO and PEO in the PEO/maleated starch blends

C.1.1 Data for Figure 4.11

log[-ln(1-X_t)]	log(t-t_0)				
	43.0 ℃	44.0 ℃	45.0 ℃	46.0 ℃	47.0 ℃
-1.2899	-0.6576	-0.5086	-0.3188	-0.2596	0.0334
-0.9773	-0.4437	-0.3098	-0.1427	-0.0506	0.1959
-0.7891	-0.3279	-0.1938	-0.0362	0.0645	0.2900
-0.6514	-0.2441	-0.1135	0.0414	0.1461	0.3598
-0.5411	-0.1739	-0.0458	0.1038	0.2148	0.4166
-0.4477	-0.1135	0.0128	0.1553	0.2695	0.4639
-0.3657	-0.0605	0.0607	0.2014	0.3201	0.5065
-0.2917	-0.0177	0.1038	0.2430	0.3636	0.5453
-0.2234	0.0294	0.1461	0.2833	0.4065	0.5809
-0.1592	0.0682	0.1875	0.3201	0.4456	0.6160
-0.0977	0.1106	0.2227	0.3560	0.4829	0.6503
-0.0380	0.1492	0.2601	0.3927	0.5211	0.6839
0.0211	0.1875	0.2989	0.4281	0.5587	0.7177
0.0806	0.2279	0.3365	0.4654	0.5977	0.7528
0.1419	0.2695	0.3766	0.5038	0.6395	0.7903
0.2067	0.3139	0.4200	0.5465	0.6857	0.8319
0.2781	0.3655	0.4698	0.5933	0.7388	0.8785
0.3622	0.4265	0.5302	0.6513	0.8048	0.9350
0.3816	0.4409	0.5453	0.6646	0.8209	0.9484
0.4024	0.4564	0.5611	0.6794	0.8388	0.9624
0.4248	0.4728	0.5786	0.6955	0.8579	0.9777
0.4492	0.4914	0.5977	0.7118	0.8791	0.9948
0.4765	0.5132	0.6191	0.7316	0.9031	1.0133
0.5077	0.5391	0.6444	0.7528	0.9304	1.0342
0.5449	0.5717	0.6749	0.7782	0.9633	1.0584

0.5924	0.6149	0.7160	0.8089	1.0048	1.0881
0.6632	0.6875	0.7782	0.8519	1.0633	1.1281

C.1.2 Data for Figure 4.12

Crystallization temperature, T_c (°C)	Half-time of crystallization, $t_{0.5}$
40.0	1.54
41.0	2.21
42.0	2.74
43.0	3.69
44.0	5.07
45.0	7.18
46.0	9.09
47.0	11.72

C.1.3 Data for Figure 4.13

Crystallization temperature, T_c (°C)	Generalized rate constant, K_A^{1/n_A}
40.0	0.506
41.0	0.360
42.0	0.289
43.0	0.218

44.0	0.156
45.0	0.110
46.0	0.085
47.0	0.071

C.1.4 Data for Figure 4.14

Crystallization temperature, T_c (°C)	log ($t_{0.5}^{-1}$)	log (K_A^{1/n_A})
40.0	-0.1875	-0.2954
41.0	-0.3444	-0.4443
42.0	-0.4378	-0.5394
43.0	-0.5670	-0.6615
44.0	-0.7050	-0.8066
45.0	-0.8561	-0.9575
46.0	-0.9586	-1.0717
47.0	-1.0689	-1.1482

C.1.5 Data for Figure 4.15

Weight fraction of acetylated rice starch	$t_{0.5}^{-1}$ (min)				
	40.0 ℃	41.0 ℃	42.0 ℃	43.0 ℃	44.0 ℃
0.0	2.2883	1.8868	1.7300	1.4925	1.1494
0.1	1.5873	1.3514	1.0638	0.8547	0.6494
0.2	1.5152	1.2500	1.0204	0.7813	0.5780
0.3	0.6494	0.4525	0.3650	0.2710	0.1972
0.4	0.3623	0.2090	0.1374	0.0880	0.0669
0.5	0.2994	0.1946	0.1030	0.0727	0.0514

APPENDIX D

D.1 Data for the estimation of equilibrium melting temperature, T_m° of pure PEO and PEO in the PEO/acetylated rice starch blends

D.1.1 Data for Figure 4.16

Crystallization temperature, T_c (°C)	Observed melting temperature, T_m (°C)		
	100/0	80/20	60/40
40	-	59.2	57.8
41	61.3	59.3	58.2
42	61.5	59.7	58.3
43	61.7	59.8	58.8
44	-	60.2	59.2
45	62.0	60.5	59.7

APPENDIX E

E.1 Data for the determination of nucleation parameter, K_g for isothermal polymer crystallization

E.1.1 Data for Figure 4.17

$T_m^\circ / (T_c\ \Delta T)$	$\ln t_{0.5}^{-1}$
0.0643	0.8278
0.0653	0.6368
0.0665	0.6162
0.0679	0.4005
0.0694	0.1393
0.0712	-0.0953
0.0732	-0.3716
0.0756	-0.7178

APPENDIX F

F.1 Nishi-Wang plot for PEO/acetylated rice starch blends

F.1.1 Data and calculation for Nishi-Wang plot of PEO/acetylated rice starch blends

$$\left(\frac{1}{T_m^o(PEO)} - \frac{1}{T_m^o(blend)}\right) = \frac{Rv_1}{\Delta H^o v_2} \chi_{12} \phi_2^2$$

$$\phi_2^2 = \left(\frac{w}{w+(1-w)(\frac{\rho_{starch}}{\rho_{PEO}})}\right)^2$$

T_m° (PEO) = 338.42 K

R = 8.314 J mol^{-1} K^{-1}

ΔH° = 7600 J mol^{-1} K^{-1}

Density of starch, ρ_{starch} = 1.5 g/cm^3

Density of PEO, ρ_{PEO} = 1.09 g/cm^3

v_1 (PEO) = $\frac{molar\ mass\ of\ repeating\ unit}{density\ of\ polymer}$

= $\frac{44.053\ g/mol}{1.09\ g/cm^3}$

= 40.42 cm^3/mol

v_2 (starch) = $\frac{molar\ mass\ of\ repeating\ unit}{density\ of\ polymer}$

= $\frac{162.14\ g/mol}{1.5\ g/cm^3}$

= 108.094 cm^3/mol

PEO/acetylated rice starch blend	Weight fraction of starch, *w*	T_m° (blend) (K)
90/10	0.1	342.29
80/20	0.2	339.06
70/30	0.3	338.91
60/40	0.4	340.88
50/50	0.5	336.10

F.1.2 Data for Figure 4.18

PEO/acetylated rice starch blend	ϕ_2^2	$\left(\frac{1}{T_m^o(PEO)} - \frac{1}{T_m^o(blend)}\right)$
90/10	0.00558	-3.341E-05
80/20	0.02364	-5.578E-06
70/30	0.05640	-4.360E-06
60/40	0.10652	-2.132E-05
50/50	0.17714	2.040E-05

F.1.3 Calculation for polymer-polymer interaction parameter, χ_{12} of PEO/acetylated rice starch blends

$$\left(\frac{1}{T_m^o(PEO)} - \frac{1}{T_m^o(blend)}\right) = \frac{Rv_1}{\Delta H^o v_2} \chi_{12} \phi_2^2$$

slope, m = $\frac{Rv_1}{\Delta H^o v_2} \chi_{12}$

χ_{12} = m × $\frac{\Delta H^o v_2}{Rv_1}$

$$= 0.0002 \times \frac{7600 \text{ J mol}^{-1} \text{ K}^{-1} \left(108.094 \frac{\text{cm}^3}{\text{mol}}\right)}{8.314 \text{ J mol}^{-1} \text{ K}^{-1} \left(40.42 \frac{\text{cm}^3}{\text{mol}}\right)}$$

$$= 0.489$$